
Dual Feature Reduction for the Sparse-Group Lasso and its Adaptive Variant

Fabio Feser

Department of Mathematics
Imperial College London
London, SW7 2AZ
ff120@ic.ac.uk

Marina Evangelou

Department of Mathematics
Imperial College London
London, SW7 2AZ
m.evangelou@ic.ac.uk

Abstract

The sparse-group lasso performs both variable and group selection, making simultaneous use of the strengths of the lasso and group lasso. It has found widespread use in genetics, a field that regularly involves the analysis of high-dimensional data, due to its sparse-group penalty, which allows it to utilize grouping information. However, the sparse-group lasso can be computationally more expensive than both the lasso and group lasso, due to the added shrinkage complexity, and its additional hyper-parameter that needs tuning. In this paper a novel dual feature reduction method, Dual Feature Reduction (DFR), is presented that uses strong screening rules for the sparse-group lasso and the adaptive sparse-group lasso to reduce their input space before optimization. DFR applies two layers of screening and is based on the dual norms of the sparse-group lasso and adaptive sparse-group lasso. Through synthetic and real numerical studies, it is shown that the proposed feature reduction approach is able to drastically reduce the computational cost in many different scenarios.

1 Introduction

High-dimensional datasets, where the number of features (p) is far greater than the number of observations (n) in a *data matrix* $\mathbf{X} \in \mathbb{R}^{n \times p}$, are becoming increasingly common with the increased rate of data collection. Applying traditional regression approaches to high-dimensional data is troublesome; the ordinary least squares solution does not have a solution if $p > n$, as it requires evaluation of $(\mathbf{X}^\top \mathbf{X})^{-1}$, which is singular in this case [16]. To alleviate this, models such as ridge [18], the lasso [44], elastic-net [56], and SLOPE [3] have been proposed and found increased use in the machine learning community [1, 24, 29, 43]. These models fall under the umbrella of *shrinkage methods*, as the estimated coefficients are shrunk towards zero during optimization, overcoming the singularity issue of the data matrix. Of the many shrinkage methods, the lasso has found the most widespread use, due to its ability to shrink coefficients exactly to zero, performing *variable selection*.

Variable selection allows a researcher to determine which features have an association with the *response* $y \in \mathbb{R}^n$. This is particularly useful in genetics, where a biological researcher may wish to discover a candidate list of genes with an association to a disease outcome. These genes can then be examined in more detail through biological experiments. However, genes are naturally found in pathways (groups of genes) and any regression approach that does not use this grouping information would not be making full use of the information available. Attempts to incorporate grouping information, leading to *group selection*, can be found through methods such as the group lasso [53], group SLOPE [5], and group SCAD [15]. However, applying only group shrinkage can lead to issues with convergence and poor predictive performance, as the model is forced to keep

all variables within an active group, leading to many noisy variables being part of the optimization process [13, 42].

The limitations of group-based regression models led to the development of sparse-group shrinkage models, such as the sparse-group lasso (SGL) [42] and sparse-group SLOPE (SGS) [13], which apply shrinkage on both variables and groups to yield concurrent variable and group selection. In particular, SGL has found increased popularity in applications in the machine learning [46, 52] and healthcare [12, 35, 42] communities, due to its ability to shrink whole groups of variables to zero, as well as variables within active groups.

To formally define SGL, suppose the variables sit within a grouping structure, where $\mathcal{G}_1, \dots, \mathcal{G}_m$ denote the disjoint sets of variable indices for the groups, of sizes p_1, \dots, p_m . Then, SGL is a convex combination of the lasso and group lasso, given by [42]

$$\hat{\beta}_{\text{sgl}}(\lambda) = \arg \min_{\beta \in \mathbb{R}^p} \{f(\beta) + \lambda \|\beta\|_{\text{sgl}}\}, \quad (1)$$

where f is the loss function, $\lambda > 0$ defines the level of shrinkage, and for $\alpha \in [0, 1]$

$$\|\beta\|_{\text{sgl}} = \alpha \|\beta\|_1 + (1 - \alpha) \sum_{g=1}^m \sqrt{p_g} \|\beta^{(g)}\|_2, \quad (2)$$

where $\beta^{(g)} \in \mathbb{R}^{p_g}$ is the vector of coefficients in group g . SGL has been extended to have adaptive shrinkage through the adaptive sparse-group lasso (aSGL) [28].

1.1 Feature reduction approaches for the sparse-group lasso

The benefits of SGL often come at the cost of increased computational cost. SGL requires the tuning of two hyper-parameters: λ , which sets the amount of shrinkage, and α , which determines the balance between the ℓ_1 and ℓ_2 penalties. Typically, α is set subjectively (Simon et al. [42] suggest $\alpha = 0.95$) and λ is tuned along a path of values $\lambda_1 \geq \dots \geq \lambda_l \geq 0$, which generates a pathwise solution of l models. Algorithms such as the Least Angle Regression (LARS) algorithm are able to calculate solutions for all possible values of λ , but are very sensitive to multicollinearity and scale quadratically, rendering their use in high-dimensional settings limited [8].

Practically, λ tends to be tuned along a path using cross-validation, magnifying the computational burden of sparse-group models. Feature reduction techniques (also called screening rules) discard features before the optimization process that would have been inactive at the optimal solution. Whilst methods exist to discard observations [41, 55], the focus of this manuscript is high-dimensional settings, in which discarding features is more impactful on computational savings.

There are two types of feature reduction techniques: *exact* and *heuristic*. Exact techniques are guaranteed to only discard inactive features, but tend to be more conservative. On the other hand, heuristic methods often discard more features, but can make mistakes [45]. These mistakes are protected against by checking the Karush–Kuhn–Tucker (KKT) optimality conditions and adding any offending features back into the optimization [21].

Most feature reduction techniques are model-specific, as they tend to make use of the KKT conditions. Exact methods were initially introduced for the lasso by the Safe Feature Elimination (SAFE) method [9], which was further extended to the group lasso [4] and sparse-group lasso [31]. Other exact examples include the dome test [51], Dual Polytope Projections (DPP) [48], and Slores [49]. The strong rule by Tibshirani et al. [45] provides a framework for applying heuristic feature reduction to penalized models with single separable norms, which has been extended to single non-separable norms in Larsson et al. [23] and sparse-group non-separable norms in Feser and Evangelou [14]. Other heuristic techniques include Sure Independence Screening (SIS) [11] and the Hessian rule [22].

Aside from the exact and heuristic categories, feature reduction techniques tend to follow three forms; *static*, where the feature reduction occurs only once (at the start of the optimization) [9, 50, 51], *dynamic*, where the reduction occurs iteratively [4], and *sequential*, where information from the previous solution is used [22, 23, 45].

An exact feature reduction method for SGL was proposed by Ndiaye et al. [31], called the GAP safe rules. The method combines sequential and dynamic feature reduction, and creates feasible regions in which active variables sit using the duality gap. GAP safe applies two layers of reduction, discarding

inactive groups and inactive variables within active groups. Other SGL exact methods are Two-layer Feature Reduction (TLFre) [47], although this was in fact shown not to be exact [30]. A heuristic approach for SGL was introduced by Liang et al. [27], called sparsegl, which is a strong rule that applies only group-level reduction. There have been other attempts to speed up SGL; Ida et al. [19] calculate approximate bounds for the inactive conditions derived in Simon et al. [42], and Li et al. [26] derive a heuristic screening rule, but it is limited to multi-response Cox models.

1.2 Contributions

In this manuscript, we propose a new dual feature reduction method for SGL and adaptive SGL: *Dual Feature Reduction* (DFR), which is based on the strong rule [45] and the bi-level framework for SGS [14]. DFR is a strong (heuristic) sequential screening rule which applies two layers of screening; it discards inactive groups and then discards inactive variables within any remaining active groups. By reducing the input dimensionality before optimization, expanded tuning regimes can be performed, including concurrent tuning of λ and α , thus overcoming the limitation of choosing α subjectively.

DFR is described for SGL in Section 2.3 and then expanded to adaptive SGL in Section 2.5. The proofs of the propositions presented in these sections are provided in Appendix A.1 for SGL and Appendix B.2 for aSGL.

2 Theory

2.1 Problem statement

SGL is fitted along a path of shrinkage parameters $\lambda_1 \geq \dots \geq \lambda_l \geq 0$. The objective is to use the solution at λ_k to generate a set of *candidate variables* $\mathcal{C}_v(\lambda_{k+1}) \subset \{1, \dots, p\}$, that is a superset of the (unknown) set of active variables at λ_{k+1} , given by $\mathcal{A}_v(\lambda_{k+1}) := \{i \in \{1, \dots, p\} : \hat{\beta}_i(\lambda_{k+1}) \neq 0\}$. The optimization at λ_{k+1} (Equation 1) is then calculated using only $\mathcal{C}_v(\lambda_{k+1})$. If the candidate set is a small proportion of the total input space, then large computational savings are expected.

To generate the candidate variable set, we first generate a candidate group set (Section 2.3.1), which is then used as a basis for constructing the final candidate variable set (Section 2.3.2). This is done using the dual norm of SGL.

2.2 Dual norm

DFR requires evaluating the dual norm of SGL, defined as $\|z\|_{\text{sgl}}^* := \sup\{z^\top x : \|x\|_{\text{sgl}} \leq 1\}$. The SGL norm can be expressed in terms of the dual of the ϵ -norm, as in Ndiaye et al. [31],

$$\|\beta\|_{\text{sgl}} = \sum_{g=1}^m (\alpha + (1 - \alpha)\sqrt{p_g}) \|\beta^{(g)}\|_{\epsilon_g}^* = \sum_{g=1}^m \tau_g \|\beta^{(g)}\|_{\epsilon_g}^*, \quad \text{where } \tau_g = \alpha + (1 - \alpha)\sqrt{p_g}. \quad (3)$$

The ϵ -norm, $\|x\|_{\epsilon_g}$, is defined as the unique nonnegative solution q of the equation [6]

$$\sum_{i=1}^{p_g} (|x_i| - (1 - \epsilon_g)q)_+^2 = (\epsilon_g q)^2, \quad \text{where } \epsilon_g = \frac{\tau_g - \alpha}{\tau_g}.$$

Using this, by Ndiaye et al. [31], the dual norm of SGL applied to a group g can be formulated as

$$\|\xi^{(g)}\|_{\text{sgl}}^* = \max_{g=1, \dots, m} \tau_g^{-1} \|\xi^{(g)}\|_{\epsilon_g}. \quad (4)$$

2.3 Dual feature reduction

The DFR method for SGL and aSGL is defined by the following screening reduction rules:

$$\text{SGL} \begin{cases} \text{Group reduction: } \|\nabla_g f(\hat{\beta}(\lambda_k))\|_{\epsilon_g} \leq \tau_g (2\lambda_{k+1} - \lambda_k) \implies \hat{\beta}^{(g)}(\lambda_{k+1}) \equiv \mathbf{0}, & (5) \\ \text{Variable reduction: } |\nabla_i f(\hat{\beta}(\lambda_k))| \leq \alpha (2\lambda_{k+1} - \lambda_k) \implies \hat{\beta}_i(\lambda_{k+1}) = 0. & (6) \end{cases}$$

$$\text{aSGL} \begin{cases} \text{Group reduction: } \|\nabla_g f(\hat{\beta}(\lambda_k))\|_{\epsilon'_g} \leq \gamma_g (2\lambda_{k+1} - \lambda_k) \implies \hat{\beta}^{(g)}(\lambda_{k+1}) \equiv \mathbf{0}, & (7) \\ \text{Variable reduction: } |\nabla_i f(\hat{\beta}(\lambda_k))| \leq \alpha v_i (2\lambda_{k+1} - \lambda_k) \implies \hat{\beta}_i(\lambda_{k+1}) = 0, & (8) \end{cases}$$

with ϵ'_g and γ_g defined in Section 2.5. Under $\alpha = \{0, 1\}$, the rules reduce to those of the (adaptive) group lasso and (adaptive) lasso respectively (Appendix A.4).

2.3.1 Group reduction

To generate a candidate group set, the KKT stationarity conditions [21] are used, providing conditions for an inactive group. For SGL, they are given by, for a group g at λ_{k+1} (using Equations 1 and 3)

$$\mathbf{0} \in \nabla_g f(\hat{\beta}(\lambda_{k+1})) + \tau_g \lambda_{k+1} \Theta_{g,k+1}, \quad (9)$$

where $\Theta_{g,k+1} = \partial \|\hat{\beta}(\lambda_{k+1})\|_{\epsilon_g}^*$ is the subgradient of the dual norm of the ϵ -norm at λ_{k+1} . The subgradient for an inactive group g (at zero) can be expressed by the unit ball of the dual norm: $\Theta_{g,k+1}^0 := \partial \|0\|_{\epsilon_g}^* = \{x \in \mathbb{R}^{p_g} : \|x\|_{\epsilon_g} \leq 1\}$ [40]. Plugging the unit ball into Equation 9 and applying the ϵ -norm, the subgradient can be canceled out, so the KKT conditions can be written as

$$-\nabla_g f(\hat{\beta}(\lambda_{k+1})) \in \tau_g \lambda_{k+1} \Theta_{g,k+1}^0 \stackrel{\|\cdot\|_{\epsilon_g}}{\iff} \|\nabla_g f(\hat{\beta}(\lambda_{k+1}))\|_{\epsilon_g} = \tau_g \lambda_{k+1} \|\Theta_{g,k+1}^0\|_{\epsilon_g} \leq \tau_g \lambda_{k+1}. \quad (10)$$

If the gradient were available, it would be possible to identify the active groups at λ_{k+1} exactly, using Equation 10. However, as this is not possible in practice, an approximation \mathcal{M}_g is required such that

$$\|\nabla_g f(\hat{\beta}(\lambda_{k+1}))\|_{\epsilon_g} \leq \mathcal{M}_g. \quad (11)$$

Then, the screening rule tests whether $\mathcal{M}_g \leq \tau_g \lambda_{k+1}$. If this is found to be true, it can be concluded that Equation 10 holds and so the group must be inactive. An approximation can be found by assuming that the gradient is a Lipschitz function of λ_{k+1} with respect to the ϵ -norm,

$$\|\nabla_g f(\hat{\beta}(\lambda_{k+1})) - \nabla_g f(\hat{\beta}(\lambda_k))\|_{\epsilon_g} \leq \tau_g |\lambda_{k+1} - \lambda_k|, \quad (12)$$

which is a similar assumption to the lasso strong rule [45]. Using the reverse triangle inequality gives

$$\|\nabla_g f(\hat{\beta}(\lambda_{k+1}))\|_{\epsilon_g} \leq \|\nabla_g f(\hat{\beta}(\lambda_k))\|_{\epsilon_g} + \tau_g (\lambda_k - \lambda_{k+1}) =: \mathcal{M}_g, \quad (13)$$

and a suitable approximation \mathcal{M}_g . Therefore, the strong group screening rule for SGL can be formulated by plugging the approximation from Equation 13 into Equation 11: discard a group g if

$$\|\nabla_g f(\hat{\beta}(\lambda_k))\|_{\epsilon_g} + \tau_g (\lambda_k - \lambda_{k+1}) \leq \tau_g \lambda_{k+1} \iff \|\nabla_g f(\hat{\beta}(\lambda_k))\|_{\epsilon_g} \leq \tau_g (2\lambda_{k+1} - \lambda_k).$$

Since the Lipschitz assumption can fail, KKT checks (Section 2.3.3) are performed to prevent violations. Propositions 2.1 and 2.2 formalize the theoretical and practical (DFR) group rules. The theoretical rule relies on knowledge of the gradient at $k + 1$, which is not available.

Proposition 2.1 (Theoretical SGL group screening). *For any $\lambda_{k+1}, k \in \{1, \dots, l-1\}$, the candidate set $\mathcal{C}_g(\lambda_{k+1}) = \{g \in \{1, \dots, m\} : \|\nabla_g f(\hat{\beta}(\lambda_{k+1}))\|_{\epsilon_g} > \tau_g \lambda_{k+1}\}$ recovers the exact support of the active groups for SGL. That is, $\mathcal{C}_g(\lambda_{k+1}) = \mathcal{A}_g(\lambda_{k+1}) := \{i \in \{1, \dots, m\} : \|\hat{\beta}^{(g)}(\lambda_{k+1})\|_2 \neq 0\}$.*

Proposition 2.2 (DFR-SGL group screening). *For any $\lambda_{k+1}, k \in \{1, \dots, l-1\}$, assuming that*

$$\|\nabla_g f(\hat{\beta}(\lambda_{k+1})) - \nabla_g f(\hat{\beta}(\lambda_k))\|_{\epsilon_g} \leq \tau_g |\lambda_{k+1} - \lambda_k|,$$

the candidate set $\mathcal{C}_g(\lambda_{k+1}) = \{g \in \{1, \dots, m\} : \|\nabla_g f(\hat{\beta}(\lambda_k))\|_{\epsilon_g} > \tau_g (2\lambda_{k+1} - \lambda_k)\}$ is a superset of the set of active groups for SGL. That is, $\mathcal{A}_g(\lambda_{k+1}) \subset \mathcal{C}_g(\lambda_{k+1})$.

2.3.2 Variable reduction

Group screening reduces the input dimensionality, but further reduction is possible by applying a second screening layer to the variables in the candidate groups. For an inactive variable, $i \notin \mathcal{A}_v(\lambda_{k+1})$, $i \in \mathcal{G}$, the KKT conditions are (using the SGL decomposition in Equation 2)

$$\mathbf{0} \in \nabla_i f(\hat{\beta}(\lambda_{k+1})) + \lambda_{k+1} \alpha \Phi_{i,k+1}^0 + \lambda_{k+1} (1 - \alpha) \Psi_{i,k+1}^{(g)}, \quad (14)$$

where Φ and Ψ are the subgradients of the ℓ_1 and ℓ_2 norms respectively. For an active group, the subgradient of the ℓ_2 norm is given by $\hat{\beta}_i^{(g)} / \|\hat{\beta}^{(g)}\|_2$, which vanishes for an inactive variable. So,

$$-\nabla_i f(\hat{\beta}(\lambda_{k+1})) \in \lambda_{k+1} \alpha \Phi_{i,k+1}^0 \stackrel{|\cdot|}{\iff} |\nabla_i f(\hat{\beta}(\lambda_{k+1}))| \leq \lambda_{k+1} \alpha, \quad (15)$$

where $\Phi_{i,k+1}^0 = \{x \in \mathbb{R} : |x| \leq 1\}$. This is similar to the strong screening rule for the lasso [45], scaled by α . Therefore, using the Lipschitz assumption

$$|\nabla_i f(\hat{\beta}(\lambda_{k+1})) - \nabla_i f(\hat{\beta}(\lambda_k))| \leq \alpha(\lambda_k - \lambda_{k+1}),$$

yields the strong variable screening rule for SGL: discard a variable j in an active group g if

$$|\nabla_i f(\hat{\beta}(\lambda_k))| \leq \alpha(2\lambda_{k+1} - \lambda_k). \quad (16)$$

To derive Equation 14, knowledge of $\mathcal{A}_g(\lambda_{k+1})$ is required, which is not possible in practice. However, by Proposition 2.2, it is contained within the candidate set $\mathcal{C}_g(\lambda_{k+1})$, and so this is used instead as an approximation. That is, the variable screening rule (Equation 6) is applied to the groups in the candidate set. The approximation is not a concern, as the KKT checks (Section 2.3.3), which are performed for any strong screening rule, will negate any errors in the approximation.

The theoretical and practical (DFR) variable rules are formalized in Propositions 2.3 and 2.4.

Proposition 2.3 (Theoretical SGL variable screening). *For any $\lambda_{k+1}, k \in \{1, \dots, l-1\}$, the candidate set $\mathcal{C}_v(\lambda_{k+1}) = \{i \in \mathcal{G}_g \text{ for } g \in \mathcal{A}_g(\lambda_{k+1}) : |\nabla_i f(\hat{\beta}(\lambda_{k+1}))| > \lambda_{k+1}\alpha\}$ recovers the exact support of the active variables for SGL. That is, $\mathcal{C}_v(\lambda_{k+1}) = \mathcal{A}_v(\lambda_{k+1})$.*

Proposition 2.4 (DFR-SGL variable screening). *For any $\lambda_{k+1}, k \in \{1, \dots, l-1\}$, assuming that*

$$|\nabla_i f(\hat{\beta}(\lambda_{k+1})) - \nabla_i f(\hat{\beta}(\lambda_k))| \leq \alpha(\lambda_k - \lambda_{k+1}),$$

the candidate set $\mathcal{C}_v(\lambda_{k+1}) = \{i \in \mathcal{G}_g \text{ for } g \in \mathcal{A}_g(\lambda_{k+1}) : |\nabla_i f(\hat{\beta}(\lambda_k))| > \alpha(2\lambda_{k+1} - \lambda_k)\}$ is a superset of the set of active variables for SGL. That is, $\mathcal{A}_v(\lambda_{k+1}) \subset \mathcal{C}_v(\lambda_{k+1})$.

2.3.3 Karush–Kuhn–Tucker (KKT) checks

The screening rules of DFR use several Lipschitz assumptions (Propositions 2.2 and 2.4), as well as approximating the group active set by the group candidate set for the variable screening step (Section 2.3.2). When these assumptions fail, the screening rules can make mistakes and incorrectly exclude active variables. To protect against this, the KKT conditions are checked for each variable after screening. A KKT violation occurs for variable $i \in \mathcal{G}_g$ if the following equation does not hold:

$$|S(\nabla_i f(\hat{\beta}(\lambda_{k+1})), \lambda_{k+1}(1 - \alpha)\sqrt{p_g})| \leq \lambda_{k+1}\alpha, \quad (17)$$

where $S(a, b) = \text{sign}(a)(|a| - b)_+$ is the soft-thresholding operator (see Appendix A.2 for the derivation). A violating variable is added back into the optimization procedure (see Section 2.4).

2.4 Algorithm

The DFR algorithm is based on the sparse-group screening framework, proposed by Feser and Evangelou [14], and is shown in Algorithm 1. DFR applies a layer of group screening, followed by variable screening on any remaining groups, to form the candidate variable set \mathcal{C}_v . This is combined with the previously active variables to form the *optimization set*, \mathcal{O}_v , which is the input space to fit SGL on. Any variables outside the optimization set are set to zero. The KKT checks are then performed (Section 2.3.3), with any violation variables added to the optimization set. This is repeated until no violations occur.

Algorithm 1 Dual Feature Reduction (DFR) for SGL

Input: $\lambda \in \mathbb{R}^l$, $\mathbf{X} \in \mathbb{R}^{n \times p}$, $y \in \mathbb{R}^n$, $\alpha \in [0, 1]$
 compute $\hat{\beta}(\lambda_1)$ using Equation 1
for $k = 1$ **to** $l - 1$ **do**
 $\mathcal{C}_g(\lambda_{k+1}) \leftarrow$ candidate groups from Equation 5
 $\mathcal{C}_v(\lambda_{k+1}) \leftarrow$ candidate variables from Equation 6 for $i \in \mathcal{G}_g, g \in \mathcal{C}_g(\lambda_{k+1})$, and $i \notin \mathcal{A}_v(\lambda_k)$ ► Optimization set
 $\mathcal{O}_v \leftarrow \mathcal{C}_v(\lambda_{k+1}) \cup \mathcal{A}_v(\lambda_k)$
 compute $\hat{\beta}_i(\lambda_{k+1}), i \in \mathcal{O}_v$, using Equation 1
 $\mathcal{K}_v \leftarrow$ variable KKT violations for $i \notin \mathcal{O}_v$, using Equation 17 ► KKT check
 while $\text{card}(\mathcal{K}_v) > 0$ **do**
 $\mathcal{O}_v \leftarrow \mathcal{O}_v \cup \mathcal{K}_v$ ► Optimization set
 compute $\hat{\beta}_i(\lambda_{k+1}), i \in \mathcal{O}_v$, using Equation 1
 $\mathcal{K}_v \leftarrow$ variable KKT violations for $i \notin \mathcal{O}_v$ using Equation 17 ► KKT check
 end while
end for
Output: $\hat{\beta}_{\text{sgl}}(\lambda_1), \dots, \hat{\beta}_{\text{sgl}}(\lambda_l) \in \mathbb{R}^{p \times l}$

2.5 Adaptive sparse-group lasso

The *Adaptive Sparse-group Lasso* (aSGL) applies adaptive shrinkage in a sparse-group setting, achieving the oracle property in a double-asymptotic framework, and has the norm [28, 36]

$$\|\beta\|_{\text{asgl}} = \alpha \sum_{i=1}^p v_i |\beta_i| + (1 - \alpha) \sum_{g=1}^m w_g \sqrt{p_g} \|\beta^{(g)}\|_2, \quad (18)$$

where v_i and w_g are adaptive weights. It has a less straightforward, but nonetheless useful, connection to the ϵ -norm, which allows for screening rules to be derived. The aSGL norm can be rewritten as (with the derivation given in Appendix B.1)

$$\|\beta\|_{\text{asgl}} = \sum_{g=1}^m \gamma_g \|\beta^{(g)}\|_{\epsilon'_g}^*, \quad \text{where} \quad (19)$$

$$\gamma_g = \alpha \|v^{(g)}\|_1 - \frac{\alpha}{\|\beta^{(g)}\|_1} \sum_{i,j \in \mathcal{G}_g, i \neq j} v_j |\beta_i| + (1 - \alpha) w_g \sqrt{p_g}, \quad \epsilon'_g = \gamma_g^{-1} (1 - \alpha) w_g \sqrt{p_g}.$$

Using similar calculations as for SGL, the strong screening rules and KKT checks for aSGL are given by Equations 7 and 8 (see Appendix B.2 for details and formal results). Algorithm 1 is also applicable for aSGL, using the corresponding aSGL equations as replacement (Algorithm A1 in Appendix B.4). The choice of adaptive weights is described in Appendix B.3.

3 Numerical results

In this section, the efficiency and robustness of DFR is evaluated through the analysis of both synthetic and real data that capture different data characteristics. As the purpose of screening rules is to reduce the dimensions of the input space and subsequently to reduce the computational cost, the following two metrics have been used in the comparisons:

- *Improvement factor* = *no screen time* / *screen time*, which defines by how many orders the screening has improved the computational fitting time. For example, a value of two indicates it is twice as fast when using screening.
- *Input proportion* = $|\mathcal{O}_v|/p$, which defines how much of the total input space was used in the optimization. For example, a value of 0.5 indicates half the input space was used.

DFR is compared with the existing SGL screening rules `sparsegl` [27] and `GAP safe` [31]. `sparsegl`, in contrast to DFR, only performs a single layer of group screening. This rule is also based on the framework of Tibshirani et al. [45], but uses a different Lipschitz assumption, which applies only the ℓ_2 group penalty, rather than the full SGL norm (as is the case for DFR). On the other hand, `GAP safe`

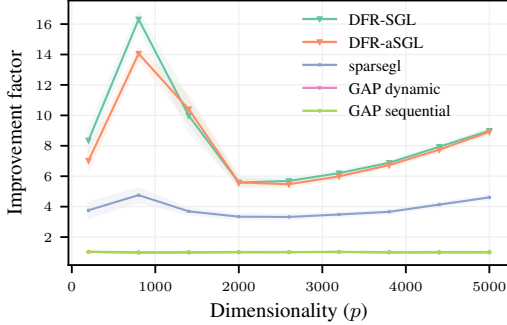


Figure 1: The *improvement factor* for strong against safe rules, applied to synthetic data under even groups of sizes 20, as a function of p , with 95% confidence intervals.

Table 1: The *improvement factor* for the strong rules applied to synthetic interaction data, with standard errors. The parameters of the synthetic data were set as $p = 400$, $n = 80$, and $m = 52$ groups of sizes in $[3, 15]$. The interaction input dimensionality was $p_{O_2} = 2111$, $p_{O_3} = 7338$ for orders 2 and 3, with no interaction hierarchy imposed. An active proportion of 0.3 was used (same signal as the marginal effects).

Method	Interaction	
	Order 2	Order 3
DFR-aSGL	137.3 ± 12.0	54.0 ± 10.7
DFR-SGL	44.3 ± 2.4	23.6 ± 3.1
sparsegl	7.4 ± 0.9	1.2 ± 0.3

is an exact feature reduction method for SGL that can be implemented dynamically or sequentially under linear regression [31]. Appendix C provides detailed descriptions of these two rules.

Throughout the analyses, the SGL optimization is performed using the Adaptive Three Operator Splitting (ATOS) [33] algorithm, although DFR can be used with any fitting algorithm.

3.1 Analysis of synthetic data

The data in this section is generated using a linear model, $y = \mathbf{X}\beta + \epsilon$, where $\mathbf{X} \sim \mathcal{N}(\mathbf{0}, \Sigma) \in \mathbb{R}^{200 \times 1000}$, the signal is sampled from $\beta \sim \mathcal{N}(0, 4)$, and the noise is $\epsilon \sim \mathcal{N}(0, 1)$. For \mathbf{X} , correlation was applied inside each group, such that $\Sigma_{i,j} = \rho = 0.3$, when i and j are in the same group. The variables were placed in $m = 22$ uneven groups of sizes in $[3, 100]$, with a 0.2 active group proportion and a 0.2 active variable proportion for variables within an active group. The models were fit along a 50-length path, starting at λ_1 (as defined by Appendix A.3 for SGL and Appendix B.2.1 for aSGL), and terminating at $0.1\lambda_1$. Each simulation case was repeated 100 times, and the presented results are averaged across these 100 repeats, unless otherwise stated. Detailed simulation set up information can be found in Appendix D.2.

Comparison to GAP safe. Comparing DFR to the GAP safe rules, it is evident that the improvement factor is significantly superior for DFR compared to both the dynamic and sequential GAP rules (Figure 1). In fact, although the input proportion of DFR and GAP safe are of similar levels (Figure A2), the cost of calculating safe regions appears to nullify any gain in dimensionality reduction. This comparison shows that the two reduction approaches (heuristic vs exact) arrive at very similar results (the screened sets), but DFR achieves this with significantly greater computational efficiency.

Increasing dimensionality. The benefits of variable screening are mostly observed in the settings of large p (Figure 1). This is further illustrated in the analysis of interaction terms (Table 1 and Appendix D.4), where within each group all possible interactions of order 2 and 3 were generated. DFR is able to improve the large computational savings when fitting interactions, especially compared to sparsegl, which under order 3 interactions provides only a marginal benefit (Table 1). These savings make it more feasible for sparse-group models to be used in interaction detection problems. Such challenges are frequently seen in the field of genetics, where gene-gene and gene-environment relationships are useful discoveries [7, 54]. Both Figure 1 and Table 1 illustrate the benefits of using bi-level screening compared to only group screening that sparsegl performs.

Robustness. A clear benefit of DFR over sparsegl is observed under very sparse signals (Figure 2). It is clear that screening rules have an increasing impact as the signal becomes sparser. However, when the signal saturates, screening approaches perform similarly, as their effectiveness is reduced. DFR is further found to be relatively unaffected by the strength of the signal and provides a benefit regardless of the strength (Figure 2). Finally, under different amounts of group correlation in \mathbf{X} , DFR is more effective at reducing the input space when compared to sparsegl, especially under minor

correlation (Figure 3). Under higher correlation, the models become less sparse, again resulting in reduced screening importance.

Across different values of α , DFR is able to effectively reduce the input space (Figure 3), with the screening efficiency a linearly decreasing function. Under values of α close to zero, SGL is forced to pick more variables within a group as active, so the input space can not be as effectively reduced. In such scenarios, the second layer of screening is not as important, shown by the similar performances of DFR and `sparsegl`. Approaching the commonly used value of $\alpha = 0.95$ shows the clear benefits of DFR. DFR-aSGL is also found to be robust under different values of γ_1 and γ_2 (Figure A6).

DFR is further shown to be effective for logistic models (Appendix D.6). The efficiency of DFR has the potential to enable approaches, like cross-validation, to be applied for the fine-tuning of all SGL and aSGL hyper-parameters, which is not often done in practice (Appendix D.7).

KKT violations. KKT violations for DFR are very rare. Across all experiments, DFR-SGL had only a single KKT violation (Table A15). Violations were more common for DFR-aSGL and `sparsegl`, but were still rare. In the experiment in which DFR-SGL had its only violation (Figure 3 (right)), DFR-aSGL had a violation every 1739 fits, and `sparsegl` had one every 53900 fits. Note that `sparsegl` violations refer to group violations, and DFR-aSGL to variable ones, making it more likely to have a variable violation. In some instances, `sparsegl` demonstrates more efficient group-level screening (Table A11), while on other occasions DFR-SGL is more efficient (Table A14). However, the elevated number of KKT violations for `sparsegl` suggests that the Lipschitz assumption of DFR is more robust.

4 Real data analysis

The efficiency of DFR is further evaluated through the analysis of six real datasets with different characteristics, including response type and input dimensionality. Three of the datasets, *brca1*, *scheetz*, and *trust-experts*, have continuous responses, so are fit using an SGL linear model. The former two were also analyzed with regards to screening rules in Larsson and Wallin [22], and the later in Liang et al. [27]. The other three datasets, *adenoma*, *celiac*, and *tumour*, have binary responses, so an SGL logistic model is used. The *trust-experts* dataset is low-dimensional, and the other five are high-dimensional. The models were fit along a 100-length path, terminating at $0.2\lambda_1$, where λ_1 generates the null model. More information on the datasets is provided in Appendix E.

For all datasets considered, DFR outperforms `sparsegl` for reducing computational cost (Figure 4) and is able to keep the *input proportion* low, even as the model saturates (Figure 5). As `sparsegl` only screens groups, when a group enters the optimization set, `sparsegl` is forced to fit with the full group.

Even in the case of low-dimensional data (*trust-experts*), DFR provides a clear benefit. DFR-aSGL performs very well for *trust-experts* and *celiac*, improving the computational cost by over 1000 times. Part of the increased efficiency over DFR-SGL in these cases is that the active sets for aSGL models tend to be smaller (Table A39), due to the increased penalization that comes with the adaptivity, which leads to the optimization set being a smaller proportion of the input space. However, despite the advantages of screening in an adaptive penalization framework, we do still observe that DFR-aSGL is more efficient at reducing the optimization set, *with respect to the active set* (Table A39).

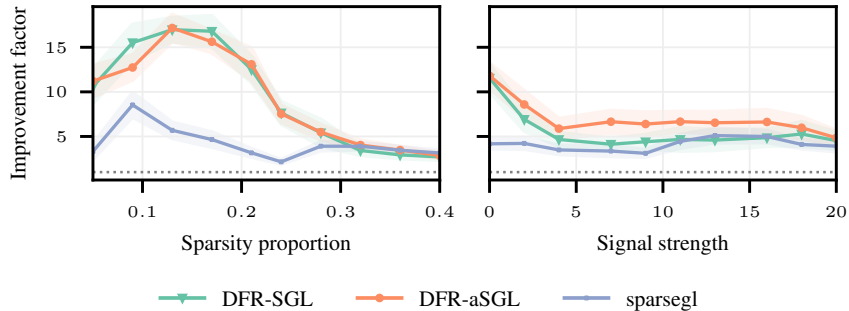


Figure 2: The *improvement factor* for the screening methods applied to synthetic data, as a function of the data sparsity proportion (left) and signal strength (right), with 95% confidence intervals.

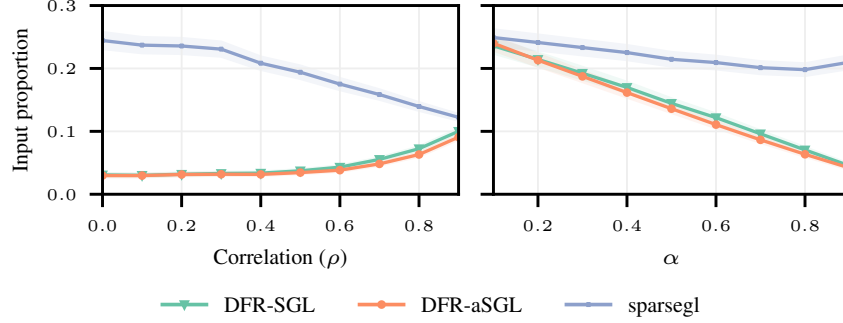


Figure 3: The *input proportion* for the screening methods applied to synthetic data, as a function of the data correlation (left) and α (right), with 95% confidence intervals.

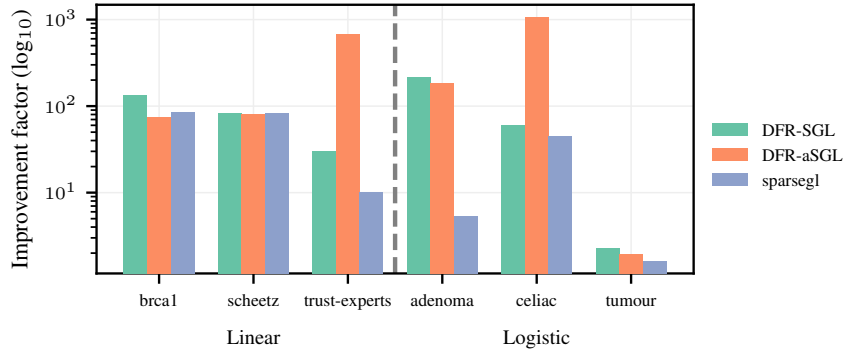


Figure 4: The *improvement factor* (\log_{10} scale) of the screening methods applied to the six real datasets, split into the model type.

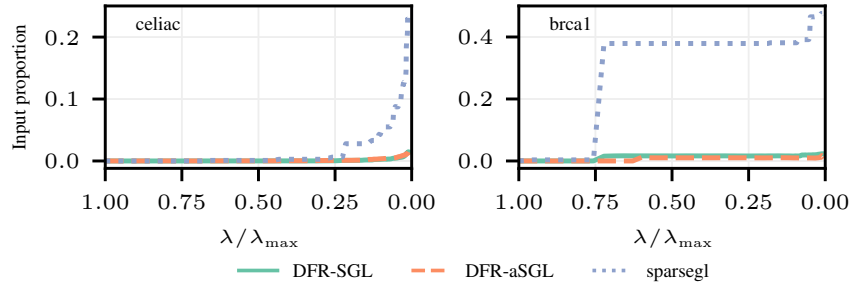


Figure 5: The *input proportion* as a function of the shrinkage path for the screening methods applied to the *celiac* and *brca1* datasets, using logistic models.

DFR is observed with aiding in mitigating convergence issues (Table A40). Across all datasets, DFR encountered no failed convergences. In contrast, *sparsegl* did not converge at several path points for both *adenoma* and *scheetz*. Applying no screening led to SGL not converging for *adenoma*, *scheetz*, and *tumour*. By drastically reducing the input space, convergence issues arising from large datasets are resolved, which not only improves computational cost, but also solution optimality.

5 Discussion

A new feature reduction approach for the sparse-group lasso and adaptive sparse-group lasso has been introduced, called *Dual Feature Reduction*. DFR applies two layers of reduction, using strong screening rules, to efficiently reduce the input dimensionality for optimization. The rules are derived using the dual norm of SGL. DFR first applies group-level screening, discarding inactive groups, followed by variable-level reduction, where inactive variables in active groups are removed.

By discarding variables that would have been inactive at the optimal solution, DFR is able to achieve significant computational savings, allowing the SGL family of models to be more efficiently implemented and applied to larger and more complex datasets. This gain comes at no cost, as the optimal solution is still achieved (Appendices D.3, D.6, and E.2). In fact, by reducing the input dimensionality, instances were observed where DFR helped SGL overcome convergence issues that would have occurred otherwise.

DFR proved robust across different data and model parameters, achieving drastic feature reduction under all scenarios considered. This consistently translated into large computational savings across both real and synthetic data. DFR also outperformed the group-level strong rule for SGL, `sparsegl`, under all considered situations, showing the benefit of applying two layers of screening.

Limitations. Several assumptions were required to perform two layers of feature reduction for SGL and aSGL. These assumptions were only broken once for SGL across all our simulations and only very infrequently for aSGL. However, it is possible that there are scenarios that we did not consider where the assumptions break down. This is a limitation of any strong screening rule, although DFR in particular carries additional assumptions over other strong rules, due to the second layer of screening.

References

- [1] Ahmed Alaoui and Michael W Mahoney. Fast Randomized Kernel Ridge Regression with Statistical Guarantees. In C Cortes, N Lawrence, D Lee, M Sugiyama, and R Garnett, editors, *Advances in Neural Information Processing Systems*, volume 28. Curran Associates, Inc., 2015.
- [2] Heinz H. Bauschke and Patrick L. Combettes. *Convex Analysis and Monotone Operator Theory in Hilbert Spaces*. Springer International Publishing, Cham, 2017. ISBN 978-3-319-48310-8. doi: 10.1007/978-3-319-48311-5.
- [3] Małgorzata Bogdan, Ewout van den Berg, Chiara Sabatti, Weijie Su, and Emmanuel J Candès. SLOPE—Adaptive variable selection via convex optimization. *The Annals of Applied Statistics*, 9(3), 2015. ISSN 1932-6157. doi: 10.1214/15-AOAS842.
- [4] Antoine Bonnefoy, Valentin Emiya, Liva Ralaivola, and Rémi Gribonval. Dynamic Screening: Accelerating First-Order Algorithms for the Lasso and Group-Lasso. *IEEE Transactions on Signal Processing*, 63(19):5121–5132, 2015. doi: 10.1109/TSP.2015.2447503.
- [5] Damian Brzyski, Alexej Gossmann, Weijie Su, and Małgorzata Bogdan. Group SLOPE – Adaptive Selection of Groups of Predictors. *Journal of the American Statistical Association*, 114(525):419–433, 2019. doi: 10.1080/01621459.2017.1411269.
- [6] Oleg Burdakov. A new vector norm for nonlinear curve fitting and some other optimization problems. In *Mathematische Optimierung | Theorie und Anwendungen*, volume 33 of *Int. Wiss. Kolloq. Fortschrreihe*, pages 15–17, 1988.
- [7] Gina M D’Angelo, DC Rao, and C Charles Gu. Combining least absolute shrinkage and selection operator (LASSO) and principal-components analysis for detection of gene-gene interactions in genome-wide association studies. *BMC Proceedings*, 3(S7):S62, 2009. ISSN 1753-6561. doi: 10.1186/1753-6561-3-S7-S62.
- [8] Bradley Efron, Trevor Hastie, Iain Johnstone, and Robert Tibshirani. Least angle regression. *The Annals of Statistics*, 32(2):407–499, 2004. doi: 10.1214/009053604000000067.
- [9] Laurent El Ghaoui, Vivian Viallon, and Tarek Rabbani. Safe feature elimination in sparse supervised learning. Technical Report UCB/EECS-2010-126, EECS Department, University of California, Berkeley, 2010.
- [10] Katarzyna A. Ellsworth, Bruce W. Eckloff, Liang Li, Irene Moon, Brooke L. Fridley, Gregory D. Jenkins, Erin Carlson, Abra Brisbin, Ryan Abo, William Bamlet, Gloria Petersen, Eric D. Wieben, and Liewei Wang. Contribution of FKBP5 Genetic Variation to Gemcitabine Treatment and Survival in Pancreatic Adenocarcinoma. *PLoS ONE*, 8(8):e70216, 2013. ISSN 1932-6203. doi: 10.1371/journal.pone.0070216.

- [11] Jianqing Fan and Jinchi Lv. Sure independence screening for ultrahigh dimensional feature space. *Journal of the Royal Statistical Society: Series B (Statistical Methodology)*, 70(5): 849–911, 2008. doi: <https://doi.org/10.1111/j.1467-9868.2008.00674.x>.
- [12] Kuangnan Fang, Xiaoyan Wang, Shengwei Zhang, Jianping Zhu, and Shuangge Ma. Bi-level variable selection via adaptive sparse group Lasso. *Journal of Statistical Computation and Simulation*, 85(13):2750–2760, 2015. ISSN 15635163. doi: 10.1080/00949655.2014.938241.
- [13] Fabio Feser and Marina Evangelou. Sparse-group SLOPE: adaptive bi-level selection with FDR-control. *arXiv preprint arXiv:2305.09467*, 2023.
- [14] Fabio Feser and Marina Evangelou. Strong screening rules for group-based SLOPE models. *arXiv preprint arXiv:2405.15357*, 2024.
- [15] Xiao Guo, Hai Zhang, Yao Wang, and Jiang-Lun Wu. Model selection and estimation in high dimensional regression models with group SCAD. *Statistics & Probability Letters*, 103:86–92, 2015. ISSN 01677152. doi: 10.1016/j.spl.2015.04.017.
- [16] Trevor Hastie, Robert Tibshirani, and Jerome Friedman. *The Elements of Statistical Learning Data Mining, Inference, and Prediction, Second Edition*, volume 103. Springer New York, 2nd ed. 20 edition, 2009. ISBN 9780387848587.
- [17] Graham A Heap, Gosia Trynka, Ritsert C Jansen, Marcel Bruinenberg, Morris A Swertz, Lotte C Dinesen, Karen A Hunt, Cisca Wijmenga, David A vanHeel, and Lude Franke. Complex nature of SNP genotype effects on gene expression in primary human leucocytes. *BMC Medical Genomics*, 2(1):1, 2009. ISSN 1755-8794. doi: 10.1186/1755-8794-2-1.
- [18] Arthur E. Hoerl and Robert W. Kennard. Ridge Regression: Biased Estimation for Nonorthogonal Problems. *Technometrics*, 12(1):55, 1970. ISSN 00401706. doi: 10.2307/1267351.
- [19] Yasutoshi Ida, Yasuhiro Fujiwara, and Hisashi Kashima. Fast Sparse Group Lasso. In H Wallach, H Larochelle, A Beygelzimer, F d Alché-Buc, E Fox, and R Garnett, editors, *Advances in Neural Information Processing Systems*, volume 32. Curran Associates, Inc., 2019.
- [20] National Cancer Institute. The cancer genome atlas program. <https://www.cancer.gov/about-nci/organization/ccg/research/structural-genomics/tcga>. Accessed: 2024-04-20.
- [21] H W Kuhn and A W Tucker. Nonlinear programming. In *Proceedings of the Second Berkeley Symposium on Mathematical Statistics and Probability*, pages 481–492, Berkeley, Los Angeles, USA, 1950. University of California Press.
- [22] Johan Larsson and Jonas Wallin. The Hessian screening rule. In *Proceedings of the 36th International Conference on Neural Information Processing Systems*. Curran Associates Inc., 2024. ISBN 9781713871088.
- [23] Johan Larsson, Małgorzata Bogdan, and Jonas Wallin. The strong screening rule for SLOPE. In *Advances in Neural Information Processing Systems*, volume 33, pages 14592–14603. Curran Associates, Inc., 2020.
- [24] Ismael Lemhadri, Feng Ruan, Louis Abraham, and Robert Tibshirani. LassoNet: A Neural Network with Feature Sparsity. *Journal of Machine Learning Research*, 22(127):1–29, 2021.
- [25] Liang Li, Jian-Wei Zhang, Gregory Jenkins, Fang Xie, Erin E. Carlson, Brooke L. Fridley, William R. Bamlet, Gloria M. Petersen, Robert R. McWilliams, and Liewei Wang. Genetic variations associated with gemcitabine treatment outcome in pancreatic cancer. *Pharmacogenetics and Genomics*, 26(12):527–537, 2016. ISSN 1744-6872. doi: 10.1097/FPC.0000000000000241.
- [26] Ruilin Li, Christopher Chang, Johanne M Justesen, Yosuke Tanigawa, Junyang Qian, Trevor Hastie, Manuel A Rivas, and Robert Tibshirani. Fast Lasso method for large-scale and ultrahigh-dimensional Cox model with applications to UK Biobank. *Biostatistics*, 23(2):522–540, 2022. ISSN 1465-4644. doi: 10.1093/biostatistics/kxaa038.

- [27] Xiaoxuan Liang, Aaron Cohen, Anibal Solón Heinsfeld, Franco Pestilli, and Daniel J. McDonald. sparsegl: An R Package for Estimating Sparse Group Lasso. *arXiv preprint arXiv:2208.02942*, 2022.
- [28] Alvaro Mendez-Civieta, M. Carmen Aguilera-Morillo, and Rosa E. Lillo. Adaptive sparse group LASSO in quantile regression. *Advances in Data Analysis and Classification*, 15(3): 547–573, 2021. ISSN 1862-5347. doi: 10.1007/s11634-020-00413-8.
- [29] Tom Michoel. Analytic solution and stationary phase approximation for the Bayesian lasso and elastic net. In S Bengio, H Wallach, H Larochelle, K Grauman, N Cesa-Bianchi, and R Garnett, editors, *Advances in Neural Information Processing Systems*, volume 31. Curran Associates, Inc., 2018.
- [30] Eugene Ndiaye, Olivier Fercoq, Alexandre Gramfort, and Joseph Salmon. GAP Safe screening rules for sparse multi-task and multi-class models. *Advances in Neural Information Processing Systems*, 2015-January:811–819, 2015. ISSN 10495258.
- [31] Eugene Ndiaye, Olivier Fercoq, Alexandre Gramfort, and Joseph Salmon. GAP Safe Screening Rules for Sparse-Group Lasso. In *Advances in Neural Information Processing Systems*, volume 29. Curran Associates, Inc., 2016.
- [32] Eugene Ndiaye, Olivier Fercoq, Alexandre Gramfort, and Joseph Salmon. Gap Safe screening rules for sparsity enforcing penalties. *Journal of Machine Learning Research*, 18, 2016. ISSN 15337928.
- [33] Fabian Pedregosa and Gauthier Gidel. Adaptive three operator splitting. In *Proceedings of the 35th International Conference on Machine Learning*, volume 80 of *Proceedings of Machine Learning Research*, pages 4085–4094. PMLR, 2018.
- [34] Huadong Pei, Liang Li, Brooke L. Fridley, Gregory D. Jenkins, Krishna R. Kalari, Wilma Lingle, Gloria Petersen, Zhenkun Lou, and Liewei Wang. FKBP51 Affects Cancer Cell Response to Chemotherapy by Negatively Regulating Akt. *Cancer Cell*, 16(3):259–266, 2009. ISSN 15356108. doi: 10.1016/j.ccr.2009.07.016.
- [35] Jie Peng, Ji Zhu, Anna Bergamaschi, Wonshik Han, Dong-Young Noh, Jonathan R. Pollack, and Pei Wang. Regularized multivariate regression for identifying master predictors with application to integrative genomics study of breast cancer. *The Annals of Applied Statistics*, 4(1), 2010. ISSN 1932-6157. doi: 10.1214/09-AOAS271.
- [36] Benjamin Poignard. Asymptotic theory of the adaptive Sparse Group Lasso. *Annals of the Institute of Statistical Mathematics*, 72(1):297–328, 2020. ISSN 0020-3157. doi: 10.1007/s10463-018-0692-7.
- [37] Jacob Sabates-Bellver, Laurens G. Van der Flier, Mariagrazia de Palo, Elisa Cattaneo, Caroline Maake, Hubert Rehrauer, Endre Laczko, Michal A. Kurowski, Janusz M. Bujnicki, Mirco Menigatti, Judith Luz, Teresa V. Ranalli, Vito Gomes, Alfredo Pastorelli, Roberto Faggiani, Marcello Anti, Josef Jiricny, Hans Clevers, and Giancarlo Marra. Transcriptome Profile of Human Colorectal Adenomas. *Molecular Cancer Research*, 5(12):1263–1275, 2007. ISSN 1541-7786. doi: 10.1158/1541-7786.MCR-07-0267.
- [38] Joshua A. Salomon, Alex Reinhart, Alyssa Bilinski, Eu Jing Chua, Wichada La Motte-Kerr, Minttu M. Rönn, Marissa B. Reitsma, Katherine A. Morris, Sarah LaRocca, Tamer H. Farag, Frauke Kreuter, Roni Rosenfeld, and Ryan J. Tibshirani. The US COVID-19 Trends and Impact Survey: Continuous real-time measurement of COVID-19 symptoms, risks, protective behaviors, testing, and vaccination. *Proceedings of the National Academy of Sciences*, 118(51), 2021. ISSN 0027-8424. doi: 10.1073/pnas.2111454118.
- [39] Todd E. Scheetz, Kwang-Youn A. Kim, Ruth E. Swiderski, Alisdair R. Philp, Terry A. Braun, Kevin L. Knudtson, Anne M. Dorrance, Gerald F. DiBona, Jian Huang, Thomas L. Casavant, Val C. Sheffield, and Edwin M. Stone. Regulation of gene expression in the mammalian eye and its relevance to eye disease. *Proceedings of the National Academy of Sciences*, 103(39): 14429–14434, 2006. ISSN 0027-8424. doi: 10.1073/pnas.0602562103.

- [40] Ulrike Schneider and Patrick Tardivel. The Geometry of Uniqueness, Sparsity and Clustering in Penalized Estimation. *Journal of Machine Learning Research*, 23:1–36, 2022.
- [41] Atsushi Shibagaki, Masayuki Karasuyama, Kohei Hatano, and Ichiro Takeuchi. Simultaneous safe screening of features and samples in doubly sparse modeling. In *Proceedings of The 33rd International Conference on Machine Learning*, volume 48 of *Proceedings of Machine Learning Research*, pages 1577–1586. PMLR, 2016.
- [42] Noah Simon, Jerome Friedman, Trevor Hastie, and Robert Tibshirani. A Sparse-Group Lasso. *Journal of Computational and Graphical Statistics*, 22(2):231–245, 2013. ISSN 1061-8600. doi: 10.1080/10618600.2012.681250.
- [43] Ryan Thompson, Amir Dezfouli, and Robert Kohn. The Contextual Lasso: Sparse Linear Models via Deep Neural Networks. In A Oh, T Naumann, A Globerson, K Saenko, M Hardt, and S Levine, editors, *Advances in Neural Information Processing Systems*, volume 36, pages 19940–19961. Curran Associates, Inc., 2023.
- [44] Robert Tibshirani. Regression Shrinkage and Selection Via the Lasso. *Journal of the Royal Statistical Society: Series B (Methodological)*, 58(1):267–288, 1996. ISSN 00359246. doi: 10.1111/j.2517-6161.1996.tb02080.x.
- [45] Robert Tibshirani, Jacob Bien, Jerome Friedman, Trevor Hastie, Noah Simon, Jonathan Taylor, and Ryan J. Tibshirani. Strong rules for discarding predictors in lasso-type problems. *Journal of the Royal Statistical Society. Series B: Statistical Methodology*, 74(2):245–266, 2010. ISSN 13697412. doi: 10.1111/j.1467-9868.2011.01004.x.
- [46] M. Vidyasagar. Machine learning methods in the computational biology of cancer. *Proceedings of the Royal Society A: Mathematical, Physical and Engineering Sciences*, 470(2167):20140081, 2014. ISSN 1364-5021. doi: 10.1098/rspa.2014.0081.
- [47] Jie Wang and Jieping Ye. Two-Layer Feature Reduction for Sparse-Group Lasso via Decomposition of Convex Sets. *Advances in Neural Information Processing Systems*, 3:2132–2140, 2014. ISSN 10495258.
- [48] Jie Wang, Jiayu Zhou, Peter Wonka, and Jieping Ye. Lasso screening rules via dual Polytope Projection. In *Proceedings of the 26th International Conference on Neural Information Processing Systems*, volume 1, pages 1070–1078. Curran Associates Inc., 2013.
- [49] Jie Wang, Jiayu Zhou, Jun Liu, Peter Wonka, and Jieping Ye. A Safe Screening Rule for Sparse Logistic Regression. In Z Ghahramani, M Welling, C Cortes, N Lawrence, and K Q Weinberger, editors, *Advances in Neural Information Processing Systems*, volume 27. Curran Associates, Inc., 2014.
- [50] Zhen Xiang, Hao Xu, and Peter J Ramadge. Learning Sparse Representations of High Dimensional Data on Large Scale Dictionaries. In J Shawe-Taylor, R Zemel, P Bartlett, F Pereira, and K Q Weinberger, editors, *Advances in Neural Information Processing Systems*, volume 24. Curran Associates, Inc., 2011.
- [51] Zhen James Xiang and Peter J Ramadge. Fast lasso screening tests based on correlations. In *2012 IEEE International Conference on Acoustics, Speech and Signal Processing (ICASSP)*, pages 2137–2140, 2012. doi: 10.1109/ICASSP.2012.6288334.
- [52] Dani Yogatama and Noah A. Smith. Linguistic Structured Sparsity in Text Categorization. In *Proceedings of the 52nd Annual Meeting of the Association for Computational Linguistics (Volume 1: Long Papers)*, pages 786–796, Stroudsburg, PA, USA, 2014. Association for Computational Linguistics. doi: 10.3115/v1/P14-1074.
- [53] Ming Yuan and Yi Lin. Model selection and estimation in regression with grouped variables. *Journal of the Royal Statistical Society: Series B (Statistical Methodology)*, 68(1):49–67, 2006. ISSN 1369-7412. doi: 10.1111/j.1467-9868.2005.00532.x.
- [54] Natalia Zemlianskaia, W. James Gauderman, and Juan Pablo Lewinger. A Scalable Hierarchical Lasso for Gene–Environment Interactions. *Journal of Computational and Graphical Statistics*, 31(4):1091–1103, 2022. ISSN 1061-8600. doi: 10.1080/10618600.2022.2039161.

- [55] Weizhong Zhang, Bin Hong, Wei Liu, Jieping Ye, Deng Cai, Xiaofei He, and Jie Wang. Scaling Up Sparse Support Vector Machines by Simultaneous Feature and Sample Reduction. In Doina Precup and Yee Whye Teh, editors, *Proceedings of the 34th International Conference on Machine Learning*, volume 70 of *Proceedings of Machine Learning Research*, pages 4016–4025. PMLR, 2017.
- [56] Hui Zou and Trevor Hastie. Regularization and Variable Selection Via the Elastic Net. *Journal of the Royal Statistical Society Series B: Statistical Methodology*, 67(2):301–320, 2005. ISSN 1369-7412. doi: 10.1111/j.1467-9868.2005.00503.x.

Appendix

Table of Contents

A Sparse-group lasso	16
A.1 Theory	16
A.2 KKT checks	17
A.3 Path start	17
A.4 Reduction to (adaptive) lasso and (adaptive) group lasso	18
B Adaptive sparse-group lasso	19
B.1 Derivation of the connection to ϵ -norm	19
B.2 Theory	20
B.3 Choice of adaptive weights	21
B.4 Algorithm	22
C Competitive feature reduction approaches	23
D Synthetic data analysis	24
D.1 Metrics	24
D.2 Set up	24
D.3 Additional results for the linear model	25
D.4 Interaction Models	31
D.5 Adaptive SGL	33
D.6 Results for the logistic model	34
D.7 Cross-validation	41
E Real data analysis	42
E.1 Data description	42
E.2 Additional results for the real data	43

A Sparse-group lasso

A.1 Theory

A.1.1 Group reduction

Proof of Proposition 2.1. To prove the two sets are equivalent, we need to prove that for any $g \in \{1, \dots, m\}$ and $k \in \{1, \dots, l-1\}$, $g \in \mathcal{A}_g(\lambda_{k+1}) \iff g \in \mathcal{C}_g(\lambda_{k+1})$. We instead prove the contrapositive: $g \notin \mathcal{C}_g(\lambda_{k+1}) \iff g \notin \mathcal{A}_g(\lambda_{k+1})$. So,

$$\begin{aligned}
g \notin \mathcal{C}_g(\lambda_{k+1}) &\iff \|\nabla_g f(\hat{\beta}(\lambda_{k+1}))\|_{\epsilon_g} \leq \tau_g \lambda_{k+1}, && \text{by definition of the candidate set} \\
&\iff -\nabla_g f(\hat{\beta}(\lambda_{k+1})) \in \tau_g \lambda_{k+1} \Theta_{g,k+1}^0, && \text{as } \Theta_{g,k+1}^0 = \{x \in \mathbb{R}^{p_g} : \|x\|_{\epsilon_g} \leq 1\} \\
&\iff \mathbf{0} \in \nabla_g f(\hat{\beta}(\lambda_{k+1})) + \tau_g \lambda_{k+1} \Theta_{g,k+1}^0 \\
&\iff g \notin \mathcal{A}_g(\lambda_{k+1}), && \text{by the KKT conditions (Equation 9)}.
\end{aligned}$$

□

Proof of Proposition 2.2. To prove the candidate set is a superset of the active set, we need to prove that for any $g \in \{1, \dots, m\}$ and $k \in \{1, \dots, l-1\}$, $g \in \mathcal{A}_g(\lambda_{k+1}) \implies g \in \mathcal{C}_g(\lambda_{k+1})$. We instead prove the contrapositive: $g \notin \mathcal{C}_g(\lambda_{k+1}) \implies g \notin \mathcal{A}_g(\lambda_{k+1})$. First, we rewrite the Lipschitz assumption as (using the reverse triangle inequality)

$$\begin{aligned}
\|\nabla_g f(\hat{\beta}(\lambda_{k+1}))\|_{\epsilon_g} - \|\nabla_g f(\hat{\beta}(\lambda_k))\|_{\epsilon_g} &\leq \|\nabla_g f(\hat{\beta}(\lambda_{k+1})) - \nabla_g f(\hat{\beta}(\lambda_k))\|_{\epsilon_g} \leq \tau_g |\lambda_{k+1} - \lambda_k| \\
&\implies \|\nabla_g f(\hat{\beta}(\lambda_{k+1}))\|_{\epsilon_g} \leq \|\nabla_g f(\hat{\beta}(\lambda_k))\|_{\epsilon_g} + \tau_g |\lambda_{k+1} - \lambda_k|.
\end{aligned} \tag{20}$$

Now, as $g \notin \mathcal{C}_g(\lambda_{k+1})$,

$$\|\nabla_g f(\hat{\beta}(\lambda_k))\|_{\epsilon_g} \leq \tau_g (2\lambda_{k+1} - \lambda_k).$$

Plugging this into Equation 20 yields

$$\begin{aligned}
&\|\nabla_g f(\hat{\beta}(\lambda_{k+1}))\|_{\epsilon_g} \leq \tau_g (2\lambda_{k+1} - \lambda_k) + \tau_g |\lambda_{k+1} - \lambda_k| \\
&\implies \|\nabla_g f(\hat{\beta}(\lambda_{k+1}))\|_{\epsilon_g} \leq \tau_g \lambda_{k+1} \\
&\implies -\nabla_g f(\hat{\beta}(\lambda_{k+1})) \in \tau_g \lambda_{k+1} \Theta_{g,k+1}^0, && \text{as } \Theta_{g,k+1}^0 = \{x \in \mathbb{R}^{p_g} : \|x\|_{\epsilon_g} \leq 1\} \\
&\implies \mathbf{0} \in \nabla_g f(\hat{\beta}(\lambda_{k+1})) + \tau_g \lambda_{k+1} \Theta_{g,k+1}^0 \\
&\implies g \notin \mathcal{A}_g(\lambda_{k+1}), && \text{by the KKT conditions (Equation 9)}.
\end{aligned}$$

□

A.1.2 Variable reduction

Proof of Proposition 2.3. The proof strategy is similar to that of Proposition 2.1. To prove the two sets are equivalent, we need to prove that for any $i \in \mathcal{G}_g$ such that $g \in \mathcal{A}_g$, and $k \in \{1, \dots, l-1\}$, $i \in \mathcal{A}_v(\lambda_{k+1}) \iff i \in \mathcal{C}_v(\lambda_{k+1})$. We instead prove the contrapositive: $i \notin \mathcal{C}_v(\lambda_{k+1}) \iff i \notin \mathcal{A}_v(\lambda_{k+1})$. So,

$$\begin{aligned}
i \notin \mathcal{C}_v(\lambda_{k+1}) &\iff |\nabla_i f(\hat{\beta}(\lambda_{k+1}))| \leq \lambda_{k+1} \alpha, && \text{by definition of the candidate set} \\
&\iff -\nabla_v f(\hat{\beta}(\lambda_{k+1})) \in \lambda_{k+1} \alpha \Phi_{i,k+1}^0, && \text{as } \Phi_{i,k+1}^0 = \{x \in \mathbb{R} : |x| \leq 1\}, \\
&&& \text{for } i \in \mathcal{G}_g, g \in \mathcal{A}_g(\lambda_{k+1}) \\
&\iff \mathbf{0} \in \nabla_v f(\hat{\beta}(\lambda_{k+1})) + \lambda_{k+1} \alpha \Phi_{i,k+1}^0 \\
&\iff i \notin \mathcal{A}_v(\lambda_{k+1}), && \text{by the KKT conditions (Equation 14)}.
\end{aligned}$$

□

Proof of Proposition 2.4. The proof strategy is similar to that of Proposition 2.2. To prove the candidate set is a superset of the active set, we need to prove that for any $i \in \mathcal{G}_g$ such that $g \in \mathcal{A}_g$, and $k \in \{1, \dots, l-1\}$, $i \in \mathcal{A}_v(\lambda_{k+1}) \implies i \in \mathcal{C}_v(\lambda_{k+1})$. We instead prove the contrapositive:

$i \notin \mathcal{C}_v(\lambda_{k+1}) \implies i \notin \mathcal{A}_v(\lambda_{k+1})$. First, we rewrite the Lipschitz assumption as (using the reverse triangle inequality)

$$|\nabla_i f(\hat{\beta}(\lambda_{k+1}))| \leq \|\nabla_i f(\hat{\beta}(\lambda_k))\| + \alpha|\lambda_{k+1} - \lambda_k|. \quad (21)$$

Now, as $i \notin \mathcal{C}_v(\lambda_{k+1})$,

$$|\nabla_i f(\hat{\beta}(\lambda_k))| \leq \alpha(2\lambda_{k+1} - \lambda_k).$$

Plugging this into Equation 21 yields

$$\begin{aligned} |\nabla_i f(\hat{\beta}(\lambda_{k+1}))| &\leq \alpha\lambda_{k+1} \\ \implies -\nabla_i f(\hat{\beta}(\lambda_{k+1})) &\in \alpha\lambda_{k+1}\Phi_{i,k+1}^0, \text{ as } \Phi_{i,k+1}^0 = \{x \in \mathbb{R} : |x| \leq 1\} \\ \implies \mathbf{0} &\in \nabla_i f(\hat{\beta}(\lambda_{k+1})) + \alpha\lambda_{k+1}\Phi_{i,k+1}^0 \\ \implies i &\notin \mathcal{A}_v(\lambda_{k+1}), \quad \text{by the KKT conditions (Equation 9).} \end{aligned}$$

□

A.2 KKT checks

To check whether a variable $i \in \mathcal{G}_g$ has been correctly discarded, the KKT optimality conditions are checked. Equation 14 describes the condition under which a variable $i \in \mathcal{G}_g$ is inactive and can be rewritten as (by the definition of $\Phi_{i,k+1}^0$)

$$|\nabla_i f(\hat{\beta}(\lambda_{k+1})) + \lambda_{k+1}(1 - \alpha)\Psi_{i,k+1}^{(g)}| \leq \lambda_{k+1}\alpha, \quad (22)$$

where $\Psi_{k+1}^{(g)} = \{x \in \mathbb{R}^{\sqrt{p_g}} : \|x\|_2 \leq 1\}$. To satisfy Equation 22, the unknown subdifferential, $\Psi_{i,k+1}^{(g)}$, is taken to be its minimum possible value. For $x \in \Psi_{k+1}^{(g)}$, we have that

$$\begin{aligned} \|x\|_2 \leq 1 &\implies \sqrt{p_g}\|x\|_2 \leq \sqrt{p_g} \\ &\implies \|x\|_1 \leq \sqrt{p_g} \text{ by the inequality } \|x\|_1 \leq \sqrt{p_g}\|x\|_2 \\ &\implies |x_i| \leq \sqrt{p_g}. \end{aligned}$$

Hence, the values in the subdifferential are bounded by $\sqrt{p_g}$. We consider the following scenarios for Equation 22

1. $\nabla_i f(\hat{\beta}(\lambda_{k+1})) > \lambda_{k+1}(1 - \alpha)\sqrt{p_g}$: choose $x_i = -\sqrt{p_g}$.
2. $\nabla_i f(\hat{\beta}(\lambda_{k+1})) < -\lambda_{k+1}(1 - \alpha)\sqrt{p_g}$: choose $x_i = \sqrt{p_g}$.
3. $\nabla_i f(\hat{\beta}(\lambda_{k+1})) \in [-\lambda_{k+1}(1 - \alpha)\sqrt{p_g}, \lambda_{k+1}(1 - \alpha)\sqrt{p_g}]$: choose $y_i = \frac{\nabla_i f(\hat{\beta}(\lambda_{k+1}))}{\lambda_{k+1}(1 - \alpha)\sqrt{p_g}}$.

Therefore, the unknown quantity can be recovered using the soft-thresholding operator and we can rewrite Equation 22 as

$$|S(\nabla_i f(\hat{\beta}(\lambda_{k+1})), \lambda_{k+1}(1 - \alpha)\sqrt{p_g})| \leq \lambda_{k+1}\alpha.$$

A similar derivation can be found in Simon et al. [42] to derive conditions to check whether a group is non-active for SGL.

A.3 Path start

When fitting SGL along a path of values, $\lambda_1 \geq \dots \geq \lambda_l \geq 0$, λ_1 is often chosen to be the exact point at which the first predictor becomes non-zero. By Ndiaye et al. [32] and using the dual norm from Equation 4, this value is given by

$$\lambda_1 = \|\nabla f(0)\|_{\text{sgl}}^* = \max_{g=1, \dots, m} \tau_g^{-1} \|\nabla_g f(0)\|_{\epsilon_g}.$$

A.4 Reduction to (adaptive) lasso and (adaptive) group lasso

Under $\alpha = 1$ with singleton groups, SGL reduces to the lasso. In this case, no group screening occurs and the variable screening rule reduces to the lasso strong rule [45]:

$$|\nabla_i f(\hat{\beta}(\lambda_k))| < 2\lambda_{k+1} - \lambda_k.$$

Under $\alpha = 0$, SGL reduces to the group lasso. Under this scenario, the group variable screening reduces to the group lasso strong rule [45]:

$$\|\nabla_g f(\hat{\beta}(\lambda_k))\|_2 < \sqrt{p_g}(2\lambda_{k+1} - \lambda_k).$$

and no variable screening is performed. For aSGL, the rules reduce to the adaptive lasso and adaptive group lasso:

$$\text{Adaptive lasso: } |\nabla_i f(\hat{\beta}(\lambda_k))| \leq v_i(2\lambda_{k+1} - \lambda_k) \implies \hat{\beta}_i(\lambda_{k+1}) = 0.$$

$$\text{Adaptive group lasso: } \|\nabla_g f(\hat{\beta}(\lambda_k))\|_{\epsilon_{g,1}} \leq w_g \sqrt{p_g}(2\lambda_{k+1} - \lambda_k) \implies \hat{\beta}^{(g)}(\lambda_{k+1}) \equiv \mathbf{0}.$$

where $\epsilon_{g,1} = 1$ in the ϵ -norm.

B Adaptive sparse-group lasso

B.1 Derivation of the connection to ϵ -norm

The aSGL norm is given by

$$\|\beta\|_{\text{asgl}} = \alpha \sum_{i=1}^p v_i |\beta_i| + (1 - \alpha) \sum_{g=1}^m w_g \sqrt{p_g} \|\beta^{(g)}\|_2.$$

The aim is to link this norm to the ϵ -norm, in a similar way to SGL:

$$\|\beta\|_{\text{sgl}} = \sum_{g=1}^m (\alpha + (1 - \alpha) \sqrt{p_g}) \|\beta^{(g)}\|_{\epsilon_g}^*.$$

Splitting up the summation term in the adaptive lasso norm yields

$$\begin{aligned} \alpha \sum_{i=1}^p v_i |\beta_i| &= \alpha \sum_{g=1}^m \sum_{i \in \mathcal{G}_g} v_i |\beta_i| \\ &= \alpha \sum_{g=1}^m \left(\sum_{j \in \mathcal{G}_g} v_j \sum_{i \in \mathcal{G}_g} |\beta_i| - \sum_{i, j \in \mathcal{G}_g, i \neq j} v_j |\beta_i| \right) \\ &= \alpha \sum_{g=1}^m \left(\sum_{j \in \mathcal{G}_g} v_j \sum_{i \in \mathcal{G}_g} |\beta_i| - \frac{\sum_{i, j \in \mathcal{G}_g, i \neq j} v_j |\beta_i|}{\sum_{i \in \mathcal{G}_g} |\beta_i|} \sum_{i \in \mathcal{G}_g} |\beta_i| \right) \\ &= \alpha \sum_{g=1}^m \sum_{i \in \mathcal{G}_g} |\beta_i| \left(\sum_{j \in \mathcal{G}_g} v_j - \frac{\sum_{i, j \in \mathcal{G}_g, i \neq j} v_j |\beta_i|}{\sum_{i \in \mathcal{G}_g} |\beta_i|} \right) \\ &= \alpha \sum_{g=1}^m \|\beta^{(g)}\|_1 \left(\|v^{(g)}\|_1 - \frac{\sum_{i, j \in \mathcal{G}_g, i \neq j} v_j |\beta_i|}{\|\beta^{(g)}\|_1} \right). \end{aligned}$$

Hence

$$\begin{aligned} \|\beta\|_{\text{asgl}} &= \alpha \sum_{i=1}^p v_i |\beta_i| + (1 - \alpha) \sum_{g=1}^m w_g \sqrt{p_g} \|\beta^{(g)}\|_2 \\ &= \sum_{g=1}^m \left[\left(\|v^{(g)}\|_1 - \frac{\sum_{i, j \in \mathcal{G}_g, i \neq j} v_j |\beta_i|}{\|\beta^{(g)}\|_1} \right) \alpha \|\beta^{(g)}\|_1 + (1 - \alpha) w_g \sqrt{p_g} \|\beta^{(g)}\|_2 \right]. \end{aligned} \quad (23)$$

Setting

$$\gamma_g = \alpha \|v^{(g)}\|_1 - \frac{\alpha \sum_{i, j \in \mathcal{G}_g, i \neq j} v_j |\beta_i|}{\|\beta^{(g)}\|_1} + (1 - \alpha) w_g \sqrt{p_g},$$

simplifies Equation 23 to

$$\|\beta\|_{\text{asgl}} = \sum_{g=1}^m \gamma_g \left[\left(\frac{\gamma_g - (1 - \alpha) w_g \sqrt{p_g}}{\gamma_g} \right) \|\beta^{(g)}\|_1 + \left(\frac{(1 - \alpha) w_g \sqrt{p_g}}{\gamma_g} \right) \|\beta^{(g)}\|_2 \right]. \quad (24)$$

Setting

$$\epsilon'_g = \frac{(1 - \alpha) w_g \sqrt{p_g}}{\gamma_g},$$

allows Equation 24 to be written in terms of the ϵ -norm

$$\|\beta\|_{\text{asgl}} = \sum_{g=1}^m \gamma_g \left[(1 - \epsilon'_g) \|\beta^{(g)}\|_1 + \epsilon'_g \|\beta^{(g)}\|_2 \right] = \sum_{g=1}^m \gamma_g \|\beta^{(g)}\|_{\epsilon'_g}^*.$$

B.1.1 Properties of the connection to the ϵ -norm

An important aspect to note is that under $\beta^{(g)} \equiv \mathbf{0}$ for a group g , the middle term in γ_g becomes

$$\lim_{\beta^{(g)} \rightarrow 0} \left(\frac{\alpha \sum_{i,j \in \mathcal{G}_g, i \neq j} v_j |\beta_i|}{\|\beta^{(g)}\|_1} \right) = \frac{\alpha(p_g - 1)}{p_g} \sum_{i=1}^{p_g} v_i,$$

so that γ_g still exists. This can be observed by using L'Hôpital's rule and noting that for $i \in \mathcal{G}_g$,

$$\frac{\partial}{\partial \beta_i} \sum_{i \neq j} v_j |\beta_i| = \sum_{i \neq j} v_j, \quad \frac{\partial}{\partial \beta_i} \|\beta^{(g)}\|_1 = 1.$$

To see how this reduces to SGL under $v \equiv 1$ and $w \equiv 1$, note that

$$\begin{aligned} \gamma_g &= \alpha \left(p_g - \frac{\sum_{i,j \in \mathcal{G}_g, i \neq j} v_j |\beta_i|}{\|\beta^{(g)}\|_1} \right) + (1 - \alpha) \sqrt{p_g} \\ &= \alpha \left(p_g - \frac{(p_g - 1) \|\beta^{(g)}\|_1}{\|\beta^{(g)}\|_1} \right) + (1 - \alpha) \sqrt{p_g} \\ &= \alpha + (1 - \alpha) \sqrt{p_g} = \tau_g. \end{aligned}$$

To understand the cross summation term, note that for the summation we are summing over each β term $p_g - 1$ times, as the matching indices are removed, that is (for simplicity of notation, we consider \mathcal{G}_1 so that the indexing here is reset from 1)

$$\begin{aligned} \sum_{i,j \in \mathcal{G}_1, i \neq j} v_j |\beta_i| &= |\beta_1| v_2 + \dots + |\beta_1| v_{p_1} + |\beta_2| v_1 + \dots + |\beta_2| v_{p_1} + \dots + |\beta_{p_1}| v_{p_1-1} \\ &= (p_1 - 1) |\beta_1| + \dots + (p_1 - 1) |\beta_{p_1}|, \text{ by setting } v_j = 1, \forall j \in \mathcal{G}_1, \text{ for SGL} \\ &= (p_1 - 1) \sum_{i \in \mathcal{G}_1} |\beta_i| = (p_1 - 1) \|\beta^{(g)}\|_1. \end{aligned}$$

Hence, ϵ'_g also reduces to ϵ_g .

B.2 Theory

B.2.1 Path start

To find the path start for aSGL, the dual norm can not be used, as γ_g is undefined for $\beta \equiv 0$. A derivation can instead be found using a similar approach to that in Simon et al. [42], where the point is found by solving the piecewise quadratic, for each $g \in \mathcal{G}$,

$$\left\| S \left(X^{(g)\top} y/n, \lambda_g v^{(g)} \alpha \right) \right\|_2^2 - p_g w_g^2 (1 - \alpha)^2 \lambda_g^2 = 0.$$

Then, choosing $\lambda_1 = \max_g \lambda_g$ gives the path start point.

B.2.2 Group screening

To derive the group screening rule for aSGL, we compare the formulations of SGL and aSGL in terms of the ϵ -norm (Equations 3 and 19):

$$\|\beta\|_{\text{sgl}} = \sum_{g=1}^m \tau_g \|\beta^{(g)}\|_{\epsilon_g}^*, \quad \|\beta\|_{\text{asgl}} = \sum_{g=1}^m \gamma_g \|\beta^{(g)}\|_{\epsilon'_g}^*. \quad (25)$$

Therefore, the derivation for the group screening rule for aSGL is identical to that of SGL (Section 2.3.1) replacing τ_g with γ_g and $\|\cdot\|_{\epsilon_g}$ with $\|\cdot\|_{\epsilon'_g}$. The group screening rule is formalized in Propositions B.1 and B.2.

Proposition B.1 (Theoretical aSGL group screening). *For any $\lambda_{k+1}, k \in \{1, \dots, l-1\}$, the candidate set $\mathcal{C}_g(\lambda_{k+1}) = \{g \in \{1, \dots, m\} : \|\nabla_g f(\hat{\beta}(\lambda_{k+1}))\|_{\epsilon'_g} > \gamma_g \lambda_{k+1}\}$ recovers the exact support of the active groups for aSGL. That is, $\mathcal{C}_g(\lambda_{k+1}) = \mathcal{A}_g(\lambda_{k+1})$.*

Proof. The proof is identical to that of Proposition 2.1 replacing τ_g with γ_g and $\|\cdot\|_{\epsilon_g}$ with $\|\cdot\|_{\epsilon'_g}$ (see Appendix A.1.1). \square

Proposition B.2 (DFR-aSGL group screening). *For any $\lambda_{k+1}, k \in \{1, \dots, l-1\}$, assuming that*

$$\|\nabla_g f(\hat{\beta}(\lambda_{k+1})) - \nabla_g f(\hat{\beta}(\lambda_k))\|_{\epsilon'_g} \leq \gamma_g |\lambda_{k+1} - \lambda_k|,$$

the candidate set $\mathcal{C}_g(\lambda_{k+1}) = \{g \in \{1, \dots, m\} : \|\nabla_g f(\hat{\beta}(\lambda_k))\|_{\epsilon'_g} > \gamma_g(2\lambda_{k+1} - \lambda_k)\}$ is a superset of the set of active groups for aSGL. That is, $\mathcal{A}_g(\lambda_{k+1}) \subset \mathcal{C}_g(\lambda_{k+1})$.

Proof. The proof is identical to that of Proposition 2.2 replacing τ_g with γ_g and $\|\cdot\|_{\epsilon_g}$ with $\|\cdot\|_{\epsilon'_g}$ (see Appendix A.1.1). \square

B.2.3 Variable screening

The construction of the variable screening rules for aSGL is very similar to those for SGL (Section 2.3.2). The key difference is that the KKT stationary conditions for aSGL for an inactive variable in an active group are given by (in comparison to Equation 15 for SGL)

$$-\nabla_i f(\hat{\beta}(\lambda_{k+1})) \in \lambda_{k+1} \alpha v_i \Phi_{i,k+1}^0.$$

Therefore, the derivation of the rule is identical, replacing α with αv_i . The variable screening rule is formalized in Propositions B.3 and B.4.

Proposition B.3 (Theoretical aSGL variable screening). *For any $\lambda_{k+1}, k \in \{1, \dots, l-1\}$, the candidate set $\mathcal{C}_v(\lambda_{k+1}) = \{i \in \mathcal{G}_g \text{ for } g \in \mathcal{A}_g(\lambda_{k+1}) : |\nabla_i f(\hat{\beta}(\lambda_{k+1}))| > \lambda_{k+1} \alpha v_i\}$ recovers the exact support of the active variables for aSGL, that is, $\mathcal{C}_v(\lambda_{k+1}) = \mathcal{A}_v(\lambda_{k+1})$.*

Proof. The proof is identical to that of Proposition 2.3 replacing α with αv_i (see Appendix A.1.2). \square

Proposition B.4 (DFR-aSGL variable screening). *For any $\lambda_{k+1}, k \in \{1, \dots, l-1\}$, assuming that*

$$|\nabla_i f(\hat{\beta}(\lambda_{k+1})) - \nabla_i f(\hat{\beta}(\lambda_k))| \leq \alpha v_i (\lambda_k - \lambda_{k+1}),$$

the candidate set $\mathcal{C}_v(\lambda_{k+1}) = \{i \in \mathcal{G}_g \text{ for } g \in \mathcal{A}_g(\lambda_{k+1}) : |\nabla_i f(\hat{\beta}(\lambda_k))| > \alpha v_i (2\lambda_{k+1} - \lambda_k)\}$ is a superset of the set of active variables for aSGL, that is, $\mathcal{A}_v(\lambda_{k+1}) \subset \mathcal{C}_v(\lambda_{k+1})$.

Proof. The proof is identical to that of Proposition 2.4 replacing α with αv_i (see Appendix A.1.2). \square

B.2.4 KKT checks

The KKT checks for aSGL are also similar to those for SGL (Section 2.3.3): a KKT violation occurs for a variable $i \in \mathcal{G}_g$ if

$$|S(\nabla_i f(\hat{\beta}(\lambda_{k+1})), \lambda_{k+1}(1 - \alpha)w_g \sqrt{p_g})| \leq \lambda_{k+1} v_i \alpha. \quad (26)$$

B.3 Choice of adaptive weights

The adaptive weights are chosen according to Mendez-Civieta et al. [28] as

$$v_i = \frac{1}{|q_{1i}|^{\gamma_1}}, w_g = \frac{1}{\|q_1^{(g)}\|_2^{\gamma_2}},$$

where q_1 is the first principal component from performing principal component analysis on \mathbf{X} and γ_1, γ_2 are chosen by the user, often in the range $[0, 2]$. The weights are shown for $\gamma_1 = \gamma_2 = 0.1$ in Figure A1.

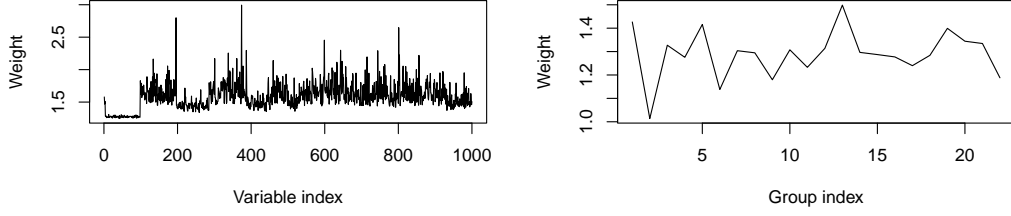


Figure A1: The weights, (v, w) , for aSGL, used in Figure 3 (left), where $p = 1000, n = 200, m = 22, \rho = 0.3, \gamma_1 = \gamma_2 = 0.1$, and $\alpha = 0.95$.

B.4 Algorithm

Algorithm A1 Dual Feature Reduction (DFR) for aSGL

Input: $\lambda \in \mathbb{R}^l, \mathbf{X} \in \mathbb{R}^{n \times p}, y \in \mathbb{R}^n, \alpha \in [0, 1]$
 compute $\hat{\beta}(\lambda_1)$ using Equation 1, replacing the SGL norm with Equation 18
for $k = 1$ **to** $l - 1$ **do**
 $\mathcal{C}_g(\lambda_{k+1}) \leftarrow$ candidate groups from Equation 7
 $\mathcal{C}_v(\lambda_{k+1}) \leftarrow$ candidate variables from Equation 8 for $i \in \mathcal{G}_g, g \in \mathcal{C}_g(\lambda_{k+1})$, and $i \notin \mathcal{A}_v(\lambda_k)$
 $\mathcal{O}_v \leftarrow \mathcal{C}_v(\lambda_{k+1}) \cup \mathcal{A}_v(\lambda_k)$ ► Optimization set
 compute $\hat{\beta}_i(\lambda_{k+1}), i \in \mathcal{O}_v$, using Equation 1, replacing the SGL norm with Equation 18
 $\mathcal{K}_v \leftarrow$ variable KKT violations for $i \notin \mathcal{O}_v$, using Equation 26 ► KKT check
 while $\text{card}(\mathcal{K}_v) > 0$ **do**
 $\mathcal{O}_v \leftarrow \mathcal{O}_v \cup \mathcal{K}_v$ ► Optimization set
 compute $\hat{\beta}_i(\lambda_{k+1}), i \in \mathcal{O}_v$, using Equation 1, replacing the SGL norm with Equation 18
 $\mathcal{K}_v \leftarrow$ variable KKT violations for $i \notin \mathcal{O}_v$, using Equation 26 ► KKT check
 end while
end for
Output: $\hat{\beta}_{\text{asgl}}(\lambda_1), \dots, \hat{\beta}_{\text{asgl}}(\lambda_l) \in \mathbb{R}^{p \times l}$

C Competitive feature reduction approaches

Sparsegl Sparsegl is a screening rule proposed by Liang et al. [27] and performs a single layer of group screening. The rule is based off the framework of Tibshirani et al. [45] and the first order condition derived in Simon et al. [42], i.e, that a group is inactive if

$$\|S(\nabla f(\beta^{(g)}), \lambda\alpha)\|_2 \leq \sqrt{p_g}(1 - \alpha)\lambda. \quad (27)$$

Using a Lipschitz assumption on the ℓ_2 norm:

$$\|\nabla_g f(\hat{\beta}(\lambda_{k+1})) - \nabla_g f(\hat{\beta}(\lambda_k))\|_2 \leq w_g(1 - \alpha)|\lambda_{k+1} - \lambda_k|, \quad (28)$$

leads to the sparsegl screening rule: discard a group g if

$$\|S(\nabla f(\beta^{(g)}), \lambda\alpha)\|_2 \leq w_g(1 - \alpha)(2\lambda_{k+1} - \lambda_k). \quad (29)$$

This screening rule uses a different Lipschitz assumption at a group-level (Equation 12), which in turn leads to a different group-level rule (Equation 5). Our Lipschitz assumption is more consistent with the work of Tibshirani et al. [45], as the assumption is with regards to the dual norm of the full SGL norm, rather than just the group lasso norm component.

GAP safe An exact feature reduction method for SGL was proposed in Ndiaye et al. [31] under linear regression. The approach makes use of the sub-differential inclusion equation of Fermat's rule [2]: $\mathbf{X}^\top \hat{\Theta}^{(\lambda, \|\cdot\|_{\text{sgl}})} \in \partial \|\cdot\|_{\text{sgl}}(\hat{\beta}^{(\lambda, \|\cdot\|_{\text{sgl}})})$, where $\hat{\Theta}$ is the solution to the dual formulation of Equation 1. Using this, exact (theoretical) rules are derived to determine which variables and groups are inactive at the optimal solution. The rules are theoretical as they rely on $\hat{\Theta}^{(\lambda, \|\cdot\|_{\text{sgl}})}$, which is not available in practice. Instead, a safe region is constructed that contains the optimal dual solution; in Ndiaye et al. [31] it is taken as a sphere, but other regions can also be used (such as domes). Due to these safe regions, the reduction is generally more conservative.

The safe region is defined as $B(\Theta_c, r)$ with radius r and center Θ_c . An ideal region would be such that r is small and the center is close to $\hat{\Theta}^{(\lambda, \|\cdot\|_{\text{sgl}})}$. Using this safe region, the GAP safe rules at λ_{k+1} are derived as

$$\text{Variable screening: } \forall j \in g, |X_j^\top \Theta_c| + r \|X_j\|_2 \leq \tau \implies \hat{\beta}_i(\lambda_{k+1}) = 0, \quad (30)$$

$$\text{Group screening: } \forall g \in \mathcal{G}, \mathcal{T}_g < (1 - \alpha)\sqrt{p_g} \implies \hat{\beta}^{(g)}(\lambda_{k+1}) = 0, \quad (31)$$

where

$$\mathcal{T}_g = \begin{cases} \|S(X_g^\top \Theta_c, \alpha)\| + r \|X_g\|, & \text{if } \|X_g^\top \Theta_c\|_\infty > \alpha, \\ (\|X_g^\top \Theta_c\|_\infty + r \|X_g\| - \alpha)_+, & \text{otherwise.} \end{cases} \quad (32)$$

The center Θ_c and the radius r are derived using the duality gap and are calculated at iteration t in an iterative algorithm as

$$\Theta_t(\beta_{(t)}) = \frac{y - \mathbf{X}\beta_{(t)}}{\max(\lambda_{k+1}, \|X^\top(y - \mathbf{X}\beta_{(t)})\|_{\text{sgl}}^*)}, \quad r_t(\beta_{(t)}, \Theta_t) = \sqrt{\frac{2P_{\lambda_{k+1}, \alpha}(\beta_{(t)}) - D_{\lambda_{k+1}}(\Theta_t)}{\lambda_{k+1}^2}}, \quad (33)$$

where $P_{\lambda, \alpha}$ and D_λ are the primal and dual objectives, and $\beta_{(t)}$ is the primal value at iteration t . The radius and center are expensive to evaluate, so are calculated every 10 iterations in Ndiaye et al. [31].

The above formulation combines both dynamic and sequential screening. The method can also be implemented using just sequential screening, in which the primal values β used in the calculation of the center and radius are from λ_k .

For both the GAP safe rules and DFR, theoretically it would be possible to exactly identify the active sets, but both instead require approximations.

D Synthetic data analysis

This section complements Section 3 by providing further information about the simulation set-up and additional results generated for the synthetic data. Additional tables and figures are provided that further showcase the effectiveness of DFR. In addition, results for synthetic data generated under the logistic model are presented. Finally, the computational savings obtained by applying screening are evaluated for cross-validation.

D.1 Metrics

The following metrics are shown in the Tables in the appendix:

- $\mathcal{A}_v, \mathcal{A}_g$: the number of active variables/groups.
- $\mathcal{C}_v, \mathcal{C}_g$: the number of variables/groups in the candidate sets.
- $\mathcal{O}_c, \mathcal{O}_g$: the number of variables/groups used in the optimization process.
- $\mathcal{K}_c, \mathcal{K}_g$: the number of variable/group KKT violations. DFR only checks for group violations and sparsegl only checks for variable violations.
- $\mathcal{O}_v / \mathcal{A}_v$ and $\mathcal{O}_g / \mathcal{A}_g$: the proportion of variables/groups used in the optimization against the number active. Defines how efficient the rules are. A low number is preferred.
- \mathcal{O}_v / p and \mathcal{O}_g / m : the variable/group input proportion, as defined in Section 3.
- ℓ_2 distance to no screen: ℓ_2 from the fitted values obtained with screening to without.

D.2 Set up

Table A1: Default model, data, and algorithm parameters for the synthetic and real data analyses.

Category	Parameter	Values	
		Synthetic	Real
Model			
	α	0.95	0.95
	$\gamma_1 = \gamma_2$ (aSGL only)	0.1	0.1
	Path length (l)	50	100
	Path termination (λ_l)	$0.1\lambda_1$	$0.2\lambda_1$
	Path shape	Log-linear	Log-linear
Data			
	p	1000	-
	n	200	-
	m	22	-
	Group sizes	[3, 100]	-
	β	$\mathcal{N}(0, 4)$	-
	Variable sparsity	0.2	-
	Group sparsity	0.2	-
	ρ	0.3	-
	ϵ	$\mathcal{N}(0, 1)$	-
Algorithm (ATOS)			
	Max iterations	5000	10000
	Backtracking	0.7	0.7
	Max backtracking iterations	100	100
	Convergence tol	10^{-5}	10^{-5}
	Standardization	ℓ_2	ℓ_2
	Intercept	Yes for linear	Yes for linear
	Warm starts	Yes	Yes

D.3 Additional results for the linear model

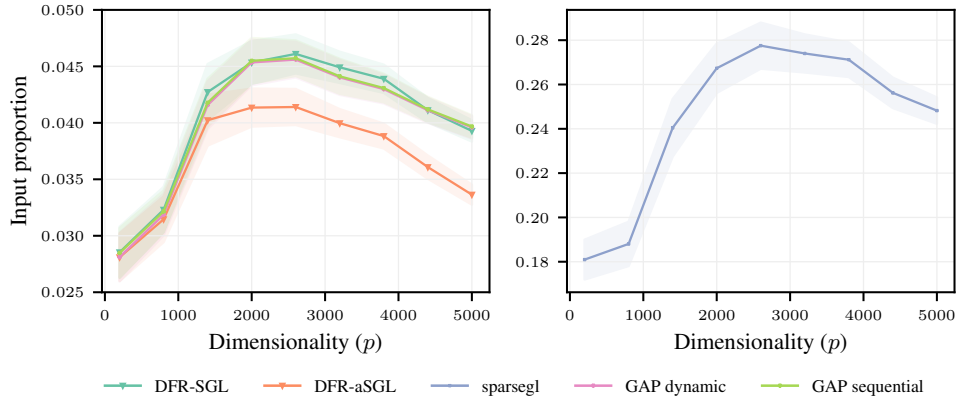


Figure A2: The *input proportion* for strong against safe rules, applied to synthetic data, as a function of the dimensionality (p), with 95% confidence intervals. sparsegl has been separated into the right plot, using a different y-scale, so that the narrow differences between the other methods can be observed.

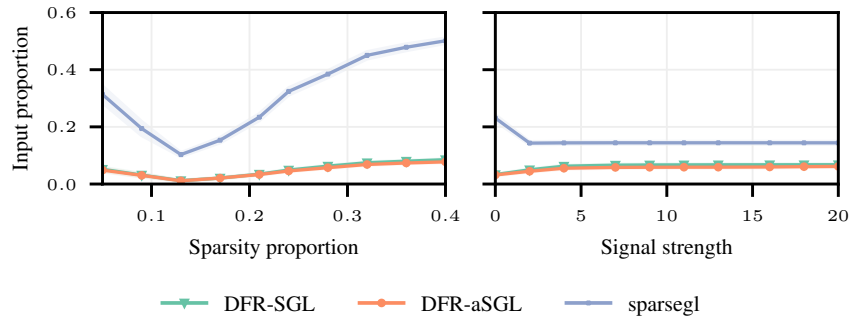


Figure A3: The *input proportion* for the screening methods applied to synthetic data, under the linear model, as a function of the data sparsity proportion (left) and signal strength (right), with 95% confidence intervals.

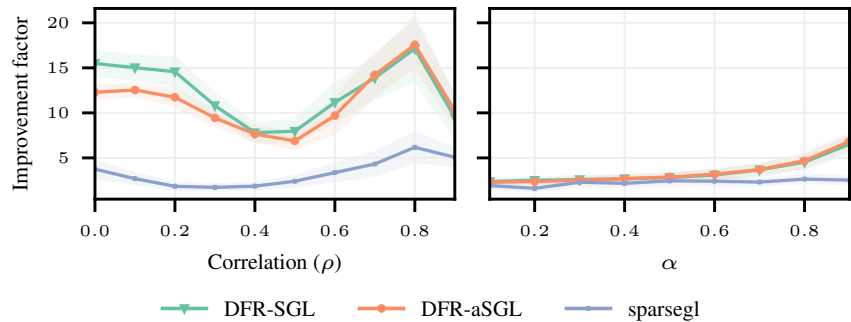


Figure A4: The *improvement factor* for the screening methods applied to synthetic data, under the linear model, as a function of the data correlation (left) and α (right), with 95% confidence intervals.

Table A2: Group screening metrics corresponding to Figure 1, averaged over all simulation iterations, dimensionality (p) cases, and path points, shown with standard errors.

METHOD	CARDINALITY			INPUT PROPORTION		
	A_g	C_g	O_g	K_g	O_g / A_g	O_g / m
DFR-ASGL	28.61 ± 0.13	36.92 ± 0.17	36.88 ± 0.17	-	1.2488 ± 0.0011	$0.1475 \pm 7 \times 10^{-4}$
DFR-SGL	28.25 ± 0.13	38.95 ± 0.18	38.95 ± 0.18	-	1.3353 ± 0.0015	$0.1558 \pm 7 \times 10^{-4}$
SPARSEGL	28.25 ± 0.13	33.64 ± 0.16	33.64 ± 0.16	$2 \times 10^{-5} \pm 2 \times 10^{-5}$	$1.142 \pm 7 \times 10^{-4}$	$0.1346 \pm 6 \times 10^{-4}$
GAP SEQUENTIAL	28.70 ± 0.13	39.00 ± 0.18	39.00 ± 0.18	-	1.3177 ± 0.0014	$0.1560 \pm 7 \times 10^{-4}$
GAP DYNAMIC	28.70 ± 0.13	39.00 ± 0.18	39.00 ± 0.18	-	1.3177 ± 0.0014	$0.1560 \pm 7 \times 10^{-4}$

Table A3: Variable screening metrics corresponding to Figure 1, averaged over all simulation iterations, dimensionality (p) cases, and path points, shown with standard errors.

METHOD	CARDINALITY			INPUT PROPORTION		
	A_v	C_v	O_v	K_v	O_v / A_v	O_v / p
DFR-ASGL	64.18 ± 0.30	36.31 ± 0.18	97.76 ± 0.47	0.1251 ± 0.0017	1.4624 ± 0.0017	$0.0196 \pm 9 \times 10^{-5}$
DFR-SGL	68.29 ± 0.32	44.70 ± 0.22	109.98 ± 0.52	0 ± 0	1.5514 ± 0.0022	$0.0220 \pm 1 \times 10^{-4}$
SPARSEGL	68.29 ± 0.32	672.82 ± 3.21	672.82 ± 3.21	-	10.1974 ± 0.0174	$0.1346 \pm 6 \times 10^{-4}$
GAP SEQUENTIAL	69.84 ± 0.33	109.36 ± 0.52	109.36 ± 0.52	-	1.5101 ± 0.0019	$0.0219 \pm 1 \times 10^{-4}$
GAP DYNAMIC	69.84 ± 0.33	109.07 ± 0.52	109.07 ± 0.52	-	1.4786 ± 0.0018	$0.0218 \pm 1 \times 10^{-4}$

Table A4: Model fitting metrics corresponding to Figure 1, averaged over all simulation iterations, dimensionality (p) cases, and path points, shown with standard errors.

METHOD	TIMINGS			ITERATIONS			ℓ_2 DISTANCE			FAILED CONVERGENCE	
	NO SCREEN (s)	SCREEN (s)	IMPROVEMENT FACTOR	NO SCREEN	SCREEN	TO NO SCREEN	NO SCREEN	SCREEN	NO SCREEN	SCREEN	
DFR-ASGL	136.53 ± 4.53	19.07 ± 0.57	7.99 ± 0.11	404.82 ± 5.85	292.99 ± 6.89	$1 \times 10^{-7} \pm 3 \times 10^{-9}$	0 ± 0	0 ± 0	0 ± 0	0 ± 0	
DFR-SGL	129.84 ± 4.2	17.86 ± 0.52	8.44 ± 0.13	395.27 ± 5.57	309.99 ± 7.05	$1 \times 10^{-10} \pm 7 \times 10^{-12}$	0 ± 0	0 ± 0	0 ± 0	0 ± 0	
SPARSEGL	129.84 ± 4.2	34.13 ± 1.04	3.86 ± 0.05	395.27 ± 5.57	387.65 ± 5.90	$9 \times 10^{-11} \pm 6 \times 10^{-12}$	0 ± 0	0 ± 0	0 ± 0	0 ± 0	
GAP SEQUENTIAL	0.77 ± 0.02	0.77 ± 0.02	1.01 ± 0.01	-	-	0 ± 0	-	-	-	-	
GAP DYNAMIC	0.77 ± 0.02	0.80 ± 0.03	0.99 ± 0.02	-	-	$3 \times 10^{-18} \pm 2 \times 10^{-18}$	-	-	-	-	

Table A5: Group screening metrics corresponding to Figure 2 (left), averaged over all simulation iterations, sparsity proportion cases, and path points, shown with standard errors.

METHOD	CARDINALITY			INPUT PROPORTION		
	\mathcal{A}_g	C_g	\mathcal{O}_g	\mathcal{K}_g	$\mathcal{O}_g / \mathcal{A}_g$	\mathcal{O}_g / m
DFR-ASGL	5.91 ± 0.03	6.62 ± 0.03	6.63 ± 0.03	–	1.1187 ± 0.0011	0.3013 ± 0.0013
DFR-SGL	5.94 ± 0.03	6.84 ± 0.03	6.84 ± 0.03	–	1.1464 ± 0.0012	0.3107 ± 0.0013
SPARSEGL	5.94 ± 0.03	6.37 ± 0.03	6.37 ± 0.03	$8 \times 10^{-5} \pm 4 \times 10^{-5}$	$1.0607 \pm 7 \times 10^{-4}$	0.2898 ± 0.0013

Table A6: Variable screening metrics corresponding to Figure 2 (left), averaged over all simulation iterations, sparsity proportion cases, and path points, shown with standard errors.

METHOD	CARDINALITY			INPUT PROPORTION		
	\mathcal{A}_v	C_v	\mathcal{O}_v	\mathcal{K}_v	$\mathcal{O}_v / \mathcal{A}_v$	\mathcal{O}_v / p
DFR-ASGL	34.62 ± 0.18	13.69 ± 0.06	46.71 ± 0.23	$0.0162 \pm 6 \times 10^{-4}$	1.3806 ± 0.002	$0.0467 \pm 2 \times 10^{-4}$
DFR-SGL	36.51 ± 0.19	15.3 ± 0.07	50.16 ± 0.25	0 ± 0	1.4017 ± 0.0022	$0.0502 \pm 2 \times 10^{-4}$
SPARSEGL	36.52 ± 0.19	313.66 ± 1.39	313.66 ± 1.39	–	12.2926 ± 0.0393	0.3137 ± 0.0014

Table A7: Model fitting metrics corresponding to Figure 2 (left), averaged over all simulation iterations, sparsity proportion cases, and path points, shown with standard errors.

METHOD	TIMINGS			ITERATIONS			ℓ_2 DISTANCE			FAILED CONVERGENCE		
	NO SCREEN (S)	SCREEN (S)	IMPROVEMENT FACTOR	NO SCREEN	SCREEN	TO NO SCREEN	NO SCREEN	SCREEN	NO SCREEN	SCREEN	NO SCREEN	SCREEN
DFR-ASGL	424.8 ± 4.6	98.0 ± 2.9	9.3 ± 0.3	248.6 ± 2.6	118.4 ± 3.2	$5 \times 10^{-8} \pm 6 \times 10^{-9}$	0 ± 0	0 ± 0	0 ± 0	0 ± 0	0 ± 0	0 ± 0
DFR-SGL	407.5 ± 4.7	106.9 ± 3.2	9.4 ± 0.3	243.1 ± 2.5	132.4 ± 3.4	$4 \times 10^{-10} \pm 2 \times 10^{-11}$	0 ± 0	0 ± 0	0 ± 0	0 ± 0	0 ± 0	0 ± 0
SPARSEGL	407.5 ± 4.7	162.0 ± 4.0	4.2 ± 0.1	243.1 ± 2.5	230.9 ± 3.0	$2 \times 10^{-10} \pm 1 \times 10^{-11}$	0 ± 0	0 ± 0	0 ± 0	0 ± 0	0 ± 0	0 ± 0

Table A8: Group screening metrics corresponding to Figure 2 (right), averaged over all simulation iterations, signal strength cases, and path points, shown with standard errors.

METHOD	CARDINALITY			INPUT PROPORTION		
	\mathcal{A}_g	\mathcal{C}_g	\mathcal{O}_g	\mathcal{K}_g	$\mathcal{O}_g / \mathcal{A}_g$	\mathcal{O}_g / m
DFR-ASGL	2.91 ± 0.01	3.04 ± 0.01	3.05 ± 0.01	-	$1.0437 \pm 7 \times 10^{-4}$	$0.1384 \pm 4 \times 10^{-4}$
DFR-SGL	2.94 ± 0.01	3.12 ± 0.01	3.12 ± 0.01	-	$1.0667 \pm 1 \times 10^{-3}$	$0.1417 \pm 4 \times 10^{-4}$
SPARSEGL	2.94 ± 0.01	3.01 ± 0.01	3.01 ± 0.01	$1 \times 10^{-4} \pm 5 \times 10^{-5}$	$1.0221 \pm 5 \times 10^{-4}$	$0.1369 \pm 3 \times 10^{-4}$

Table A9: Variable screening metrics corresponding to Figure 2 (right), averaged over all simulation iterations, signal strength cases, and path points, shown with standard errors.

METHOD	CARDINALITY			INPUT PROPORTION		
	\mathcal{A}_v	\mathcal{C}_v	\mathcal{O}_v	\mathcal{K}_v	$\mathcal{O}_v / \mathcal{A}_v$	\mathcal{O}_v / p
DFR-ASGL	38.52 ± 0.1	17.46 ± 0.04	54.86 ± 0.13	$0.0045 \pm 3 \times 10^{-4}$	1.4829 ± 0.0014	$0.0549 \pm 1 \times 10^{-4}$
DFR-SGL	42.35 ± 0.11	20.3 ± 0.05	61.48 ± 0.14	0 ± 0	1.504 ± 0.0015	$0.0615 \pm 1 \times 10^{-4}$
SPARSEGL	42.35 ± 0.11	152.75 ± 0.4	152.75 ± 0.4	-	4.4183 ± 0.016	$0.1528 \pm 4 \times 10^{-4}$

Table A10: Model fitting metrics corresponding to Figure 2 (right), averaged over all simulation iterations, signal strength cases, and path points, shown with standard errors.

METHOD	TIMINGS			ITERATIONS			ℓ_2 DISTANCE			FAILED CONVERGENCE			
	NO SCREEN (S)	SCREEN (S)	IMPROVEMENT FACTOR	NO SCREEN	SCREEN	TO NO SCREEN	TO NO SCREEN	NO SCREEN	SCREEN	NO SCREEN	SCREEN	NO SCREEN	SCREEN
DFR-ASGL	444.2 ± 4.8	113.6 ± 2.4	7.0 ± 0.2	292.8 ± 1.9	268.2 ± 3.1	$4 \times 10^{-6} \pm 3 \times 10^{-7}$	$4 \times 10^{-6} \pm 3 \times 10^{-7}$	0 ± 0	0 ± 0	0 ± 0	0 ± 0	0 ± 0	0 ± 0
DFR-SGL	181.3 ± 2.1	58.1 ± 1.2	5.6 ± 0.2	276.8 ± 1.4	255.6 ± 2.6	$5 \times 10^{-11} \pm 7 \times 10^{-12}$	$5 \times 10^{-11} \pm 7 \times 10^{-12}$	0 ± 0	0 ± 0	0 ± 0	0 ± 0	0 ± 0	0 ± 0
SPARSEGL	181.3 ± 2.1	67.7 ± 1.4	4.1 ± 0.1	276.8 ± 1.4	275.6 ± 1.5	$4 \times 10^{-11} \pm 6 \times 10^{-12}$	$4 \times 10^{-11} \pm 6 \times 10^{-12}$	0 ± 0	0 ± 0	0 ± 0	0 ± 0	0 ± 0	0 ± 0

Table A11: Group screening metrics corresponding to Figure 3 (left), averaged over all simulation iterations, correlation cases, and path points, shown with standard errors.

METHOD	CARDINALITY			INPUT PROPORTION		
	\mathcal{A}_g	\mathcal{C}_g	\mathcal{O}_g	\mathcal{K}_g	$\mathcal{O}_g / \mathcal{A}_g$	\mathcal{O}_g / m
DFR-ASGL	3.79 ± 0.01	4.31 ± 0.02	4.31 ± 0.02	-	$1.1085 \pm 1 \times 10^{-3}$	$0.1958 \pm 7 \times 10^{-4}$
DFR-SGL	3.67 ± 0.01	4.31 ± 0.02	4.31 ± 0.02	-	1.1356 ± 0.0012	$0.1959 \pm 7 \times 10^{-4}$
SPARSEGL	3.67 ± 0.01	3.98 ± 0.01	3.98 ± 0.01	$1 \times 10^{-4} \pm 5 \times 10^{-5}$	$1.0571 \pm 7 \times 10^{-4}$	$0.1809 \pm 7 \times 10^{-4}$

Table A12: Variable screening metrics corresponding to Figure 3 (left), averaged over all simulation iterations, correlation cases, and path points, shown with standard errors.

METHOD	CARDINALITY			INPUT PROPORTION		
	\mathcal{A}_v	\mathcal{C}_v	\mathcal{O}_v	\mathcal{K}_v	$\mathcal{O}_v / \mathcal{A}_v$	\mathcal{O}_v / p
DFR-ASGL	26.37 ± 0.09	17.39 ± 0.08	42.92 ± 0.16	$0.0088 \pm 4 \times 10^{-4}$	1.6214 ± 0.0026	$0.0429 \pm 2 \times 10^{-4}$
DFR-SGL	29.36 ± 0.11	18.25 ± 0.08	46.77 ± 0.17	0 ± 0	1.6025 ± 0.003	$0.0468 \pm 2 \times 10^{-4}$
SPARSEGL	29.36 ± 0.11	194.56 ± 0.78	194.56 ± 0.78	-	9.033 ± 0.0325	$0.1946 \pm 8 \times 10^{-4}$

Table A13: Model fitting metrics corresponding to Figure 3 (left), averaged over all simulation iterations, correlation cases, and path points, shown with standard errors.

METHOD	TIMINGS			ITERATIONS			ℓ_2 DISTANCE			FAILED CONVERGENCE		
	NO SCREEN (S)	SCREEN (S)	IMPROVEMENT FACTOR	NO SCREEN	SCREEN	SCREEN	TO NO SCREEN	NO SCREEN	SCREEN	NO SCREEN	NO SCREEN	SCREEN
DFR-ASGL	251.4 ± 7.9	29.4 ± 1.2	11.2 ± 0.3	825.6 ± 32.0	300.6 ± 14.6	300.6 ± 14.6	$1 \times 10^{-8} \pm 2 \times 10^{-9}$	$1 \times 10^{-8} \pm 2 \times 10^{-9}$	0 ± 0	0 ± 0	0 ± 0	
DFR-SGL	268.1 ± 10.0	35.4 ± 1.8	12.3 ± 0.3	801.6 ± 30.5	334.1 ± 16.0	334.1 ± 16.0	$5 \times 10^{-10} \pm 4 \times 10^{-11}$	$5 \times 10^{-10} \pm 4 \times 10^{-11}$	0 ± 0	0 ± 0	0 ± 0	
SPARSEGL	268.1 ± 10.0	104.8 ± 3.1	3.3 ± 0.1	801.6 ± 30.5	624.9 ± 25.8	624.9 ± 25.8	$1 \times 10^{-10} \pm 9 \times 10^{-12}$	$1 \times 10^{-10} \pm 9 \times 10^{-12}$	0 ± 0	0 ± 0	0 ± 0	

Table A14: Group screening metrics corresponding to Figure 3 (right), averaged over all simulation iterations, α cases, and path points, shown with standard errors.

METHOD	CARDINALITY			INPUT PROPORTION		
	\mathcal{A}_g	\mathcal{C}_g	\mathcal{O}_g	\mathcal{K}_g	$\mathcal{O}_g / \mathcal{A}_g$	\mathcal{O}_g / m
DFR-ASGL	3.40 ± 0.01	4.61 ± 0.02	4.61 ± 0.02	-	1.1680 ± 0.0012	$0.2094 \pm 8 \times 10^{-4}$
DFR-SGL	3.99 ± 0.01	5.37 ± 0.02	5.37 ± 0.02	-	1.1819 ± 0.0012	$0.2441 \pm 9 \times 10^{-4}$
SPARSEGL	3.99 ± 0.01	6.64 ± 0.03	6.64 ± 0.03	2×10^{-5}	1.7826 ± 0.0123	0.302 ± 0.0013

Table A15: Variable screening metrics corresponding to Figure 3 (right), averaged over all simulation iterations, α cases, and path points, shown with standard errors.

METHOD	CARDINALITY			INPUT PROPORTION		
	\mathcal{A}_v	\mathcal{C}_v	\mathcal{O}_v	\mathcal{K}_v	$\mathcal{O}_v / \mathcal{A}_v$	\mathcal{O}_v / p
DFR-ASGL	91.66 ± 0.44	61.06 ± 0.64	149.44 ± 0.80	$6 \times 10^{-4} \pm 1 \times 10^{-4}$	1.3676 ± 0.0025	$0.1494 \pm 8 \times 10^{-4}$
DFR-SGL	96.34 ± 0.44	61.15 ± 0.62	154.12 ± 0.80	$2 \times 10^{-5} \pm 2 \times 10^{-5}$	1.3546 ± 0.0022	$0.1541 \pm 8 \times 10^{-4}$
SPARSEGL	96.42 ± 0.44	305.94 ± 1.29	305.94 ± 1.29	-	20.3134 ± 0.4232	0.3059 ± 0.0013

Table A16: Model fitting metrics corresponding to Figure 3 (right), averaged over all simulation iterations, α cases, and path points, shown with standard errors.

METHOD	TIMINGS			ITERATIONS			ℓ_2 DISTANCE			FAILED CONVERGENCE		
	NO SCREEN (S)	SCREEN (S)	IMPROVEMENT FACTOR	NO SCREEN	SCREEN	SCREEN	TO NO SCREEN	NO SCREEN	SCREEN	NO SCREEN	NO SCREEN	SCREEN
DFR-ASGL	87.8 ± 1.3	33.8 ± 0.8	3.9 ± 0.1	179.6 ± 2.6	144.8 ± 2.7	$5 \times 10^{-4} \pm 4 \times 10^{-6}$	$5 \times 10^{-4} \pm 4 \times 10^{-6}$	0 ± 0	0 ± 0	0 ± 0	0 ± 0	0 ± 0
DFR-SGL	99.4 ± 1.1	35.5 ± 0.8	5.3 ± 0.2	213.6 ± 2.9	153.9 ± 2.5	$4 \times 10^{-4} \pm 3 \times 10^{-6}$	$4 \times 10^{-4} \pm 3 \times 10^{-6}$	0 ± 0	0 ± 0	0 ± 0	0 ± 0	0 ± 0
SPARSEGL	99.4 ± 1.1	75.7 ± 2.3	2.5 ± 0.1	213.6 ± 2.9	195.3 ± 3.2	$4 \times 10^{-4} \pm 3 \times 10^{-6}$	$4 \times 10^{-4} \pm 3 \times 10^{-6}$	0 ± 0	0 ± 0	0 ± 0	0 ± 0	0 ± 0

D.4 Interaction Models

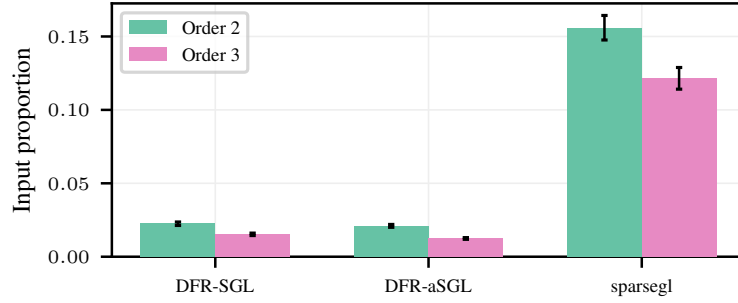


Figure A5: The *input proportion* for the strong rules applied to synthetic interaction data, under the linear model, with standard errors. The parameters of the synthetic data were set as $p = 400$, $n = 80$, and $m = 52$ groups of sizes in $[3, 15]$. The interaction input dimensionality was $p_{O_2} = 2111$, $p_{O_3} = 7338$ for orders 2 and 3, with no interaction hierarchy is imposed.

Table A17: Group screening metrics corresponding to Table 1, averaged all simulation iterations and path points, shown with standard errors.

METHOD	TYPE	CARDINALITY			INPUT PROPORTION		
		\mathcal{A}_g	\mathcal{C}_g	\mathcal{O}_g	\mathcal{K}_g	$\mathcal{O}_g / \mathcal{A}_g$	\mathcal{O}_g / m
DFR-ASGL	ORDER 2	11.3 ± 0.1	14.9 ± 0.2	14.9 ± 0.2	-	1.291 ± 0.004	0.143 ± 0.002
DFR-SGL	ORDER 2	10.9 ± 0.1	15.7 ± 0.2	15.7 ± 0.2	-	1.391 ± 0.005	0.151 ± 0.002
SPARSEGL	ORDER 2	10.9 ± 0.1	13.2 ± 0.2	13.2 ± 0.2	0 ± 0	1.166 ± 0.003	0.127 ± 0.002
DFR-ASGL	ORDER 3	7.9 ± 0.1	11.0 ± 0.2	10.9 ± 0.2	-	1.340 ± 0.005	0.105 ± 0.002
DFR-SGL	ORDER 3	8.1 ± 0.1	12.4 ± 0.2	12.4 ± 0.2	-	1.468 ± 0.006	0.119 ± 0.002
SPARSEGL	ORDER 3	8.1 ± 0.1	10.2 ± 0.2	10.2 ± 0.2	4×10^{-4}	1.203 ± 0.003	0.098 ± 0.001

Table A18: Variable screening metrics corresponding to Table 1, averaged all simulation iterations and path points, shown with standard errors.

METHOD	TYPE	CARDINALITY			INPUT PROPORTION		
		\mathcal{A}_v	\mathcal{C}_v	\mathcal{O}_v	\mathcal{K}_v	$\mathcal{O}_v / \mathcal{A}_v$	\mathcal{O}_v / p
DFR-ASGL	ORDER 2	26.5 ± 0.4	19.1 ± 0.3	44.4 ± 0.6	0.071 ± 0.004	1.617 ± 0.007	0.021 ± 0.000
DFR-SGL	ORDER 2	25.9 ± 0.4	22.8 ± 0.3	47.5 ± 0.7	0 ± 0	1.739 ± 0.009	0.023 ± 0.000
SPARSEGL	ORDER 2	25.9 ± 0.4	329.2 ± 5.0	329.2 ± 5.0	-	11.771 ± 0.097	0.156 ± 0.002
DFR-ASGL	ORDER 3	41.8 ± 0.7	51.8 ± 0.8	91.2 ± 1.5	0.047 ± 0.003	2.278 ± 0.038	0.012 ± 0.000
DFR-SGL	ORDER 3	46.2 ± 0.8	68.4 ± 1.2	111.9 ± 1.9	0 ± 0	2.712 ± 0.052	0.015 ± 0.000
SPARSEGL	ORDER 3	46.2 ± 0.8	891.5 ± 16.5	891.5 ± 16.5	-	17.886 ± 0.295	0.122 ± 0.002

Table A19: Model fitting metrics corresponding to Table 1, averaged all simulation iterations and path points, shown with standard errors.

METHOD	TYPE	TIMINGS			ITERATIONS			ℓ_2 DISTANCE			FAILED CONVERGENCE		
		No SCREEN (s)	SCREEN (s)	IMPROVEMENT FACTOR	No SCREEN	SCREEN	TO NO SCREEN	TO NO SCREEN	No SCREEN	SCREEN	No SCREEN	SCREEN	
DFR-ASGL	ORDER 2	12041 ± 411	174 ± 13	137 ± 12	1333 ± 39	137 ± 6	2×10^{-8}	2×10^{-8}	2×10^{-9}	0 ± 0	0 ± 0	0 ± 0	
DFR-SGL	ORDER 2	987 ± 48	32 ± 3	44 ± 2	1271 ± 38	140 ± 6	7×10^{-11}	7×10^{-11}	1×10^{-11}	0 ± 0	0 ± 0	0 ± 0	
SPARSEGL	ORDER 2	987 ± 48	319 ± 29	7 ± 1	1271 ± 38	658 ± 53	2×10^{-11}	2×10^{-11}	1×10^{-11}	0 ± 0	0 ± 0	0 ± 0	
DFR-ASGL	ORDER 3	12209 ± 491	877 ± 65	54 ± 11	1003 ± 33	615 ± 30	1×10^{-8}	1×10^{-8}	2×10^{-9}	0 ± 0	0 ± 0	0 ± 0	
DFR-SGL	ORDER 3	1265 ± 52	103 ± 7	24 ± 3	1089 ± 49	677 ± 32	5×10^{-11}	5×10^{-11}	6×10^{-12}	0 ± 0	0 ± 0	0 ± 0	
SPARSEGL	ORDER 3	1265 ± 52	2381 ± 170	1 ± 0.3	1089 ± 49	782 ± 33	3×10^{-11}	3×10^{-11}	4×10^{-12}	0 ± 0	0 ± 0	0 ± 0	

D.5 Adaptive SGL

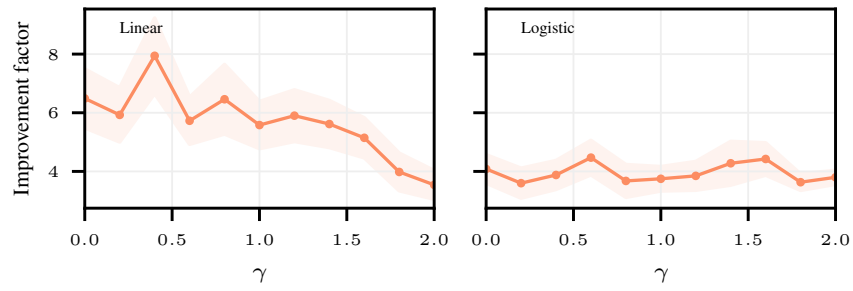


Figure A6: Robustness of DFR-aSGL under different $\gamma_1 = \gamma_2$ values for the weights, shown for linear (left) and logistic (right) models, with 95% confidence intervals. The data was generated using the parameters in Table A1.

D.6 Results for the logistic model

The data input components \mathbf{X} , β , and ϵ for the logistic model were generated as for the linear models. The class probabilities for the response were calculated using $\sigma(\mathbf{X}\beta + \epsilon)$, where σ is the sigmoid function.

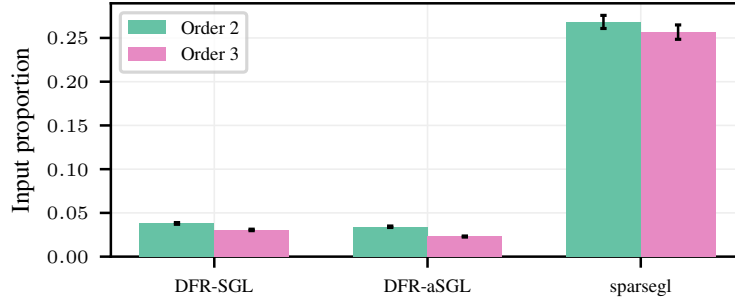


Figure A7: The *input proportion* for the strong rules applied to synthetic interaction data, under the logistic model, with standard errors. The parameters of the synthetic data were set as $p = 400$, $n = 80$, and $m = 52$ groups of sizes in $[3, 15]$. The interaction input dimensionality was $p_{O_2} = 2111$, $p_{O_3} = 7338$ for orders 2 and 3, with no interaction hierarchy is imposed.

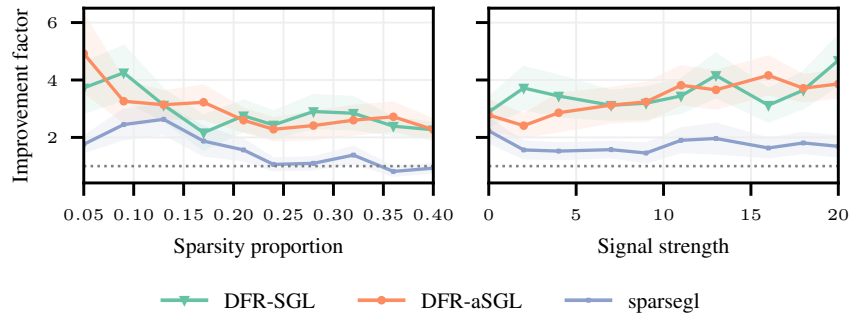


Figure A8: The *improvement factor* for the screening methods applied to synthetic data, under the logistic model, as a function of the data sparsity proportion (left) and signal strength (right), with 95% confidence intervals.

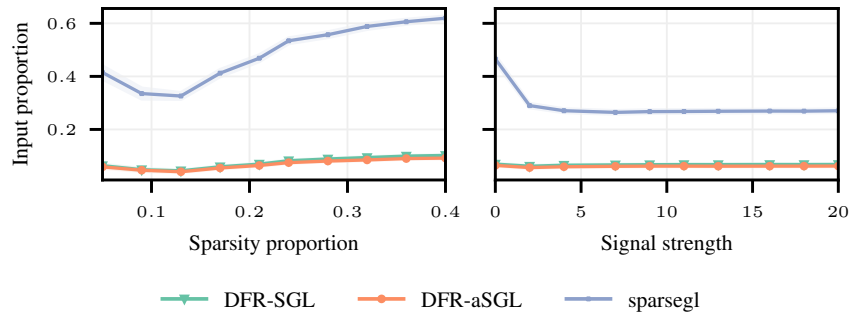


Figure A9: The *input proportion* for the screening methods applied to synthetic data, under the logistic model, as a function of the data sparsity proportion (left) and signal strength (right), with 95% confidence intervals.

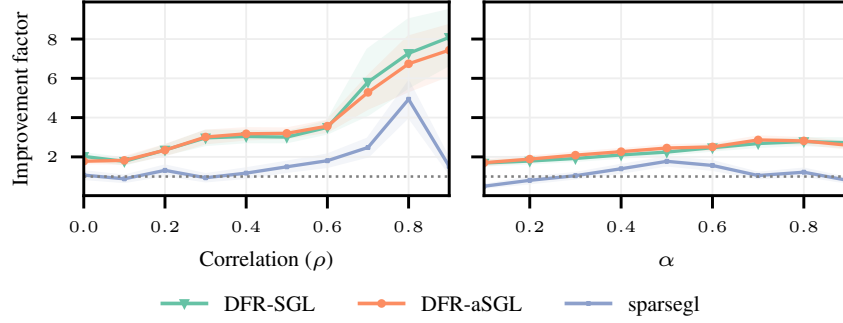


Figure A10: The *improvement factor* for the screening methods applied to synthetic data, under the logistic model, as a function of the data correlation (left) and α (right), with 95% confidence intervals.

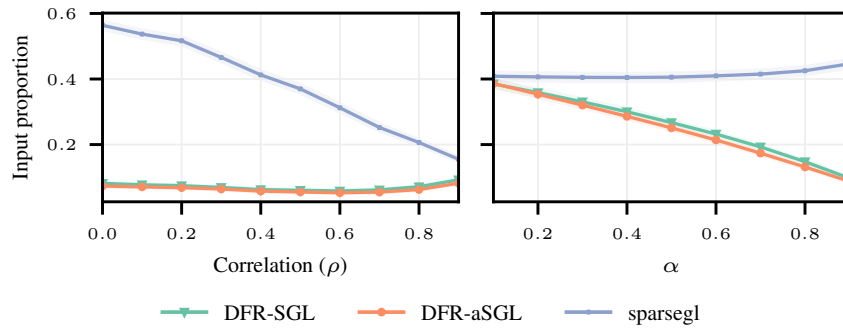


Figure A11: The *input proportion* for the screening methods applied to synthetic data, under the logistic model, as a function of the data correlation (left) and α (right), with 95% confidence intervals.

Table A20: The *improvement factor* for the strong rules applied to synthetic interaction data, under the logistic model, with standard errors. For the interaction data, the parameters of the synthetic data were set as $p = 400$, $n = 80$, and $m = 52$ groups of sizes in $[3, 15]$. The interaction input dimensionality was $p_{O_2} = 2111$, $p_{O_3} = 7338$ for orders 2 and 3, with no interaction hierarchy imposed.

Method	Interaction	
	Order 2	Order 3
DFR-aSGL	6.7 ± 0.4	12.2 ± 0.4
DFR-SGL	5.8 ± 0.2	8.3 ± 0.4
sparsegl	1.0 ± 0.1	2.1 ± 0.3

Table A21: Group screening metrics corresponding to Table A20, averaged over all simulation iterations and path points, shown with standard errors.

METHOD	TYPE	CARDINALITY			INPUT PROPORTION		
		\mathcal{A}_g	\mathcal{C}_g	\mathcal{O}_g	\mathcal{K}_g	$\mathcal{O}_g / \mathcal{A}_g$	\mathcal{O}_g / m
DFR-ASGL	ORDER 2	17.6 ± 0.2	23.1 ± 0.2	23.1 ± 0.2	-	1.320 ± 0.004	0.222 ± 0.002
DFR-SGL	ORDER 2	17.8 ± 0.2	25.0 ± 0.2	25.0 ± 0.2	-	1.419 ± 0.005	0.240 ± 0.002
SPARSEGL	ORDER 2	17.8 ± 0.2	20.9 ± 0.2	20.9 ± 0.2	2×10^{-4}	1.159 ± 0.003	0.201 ± 0.002
DFR-ASGL	ORDER 3	14.1 ± 0.2	19.9 ± 0.2	19.8 ± 0.2	-	1.396 ± 0.005	0.190 ± 0.002
DFR-SGL	ORDER 3	15.3 ± 0.2	23.7 ± 0.3	23.7 ± 0.3	-	1.525 ± 0.006	0.228 ± 0.002
SPARSEGL	ORDER 3	15.3 ± 0.2	19.3 ± 0.2	19.3 ± 0.2	2×10^{-4}	1.215 ± 0.003	0.185 ± 0.002

Table A22: Variable screening metrics corresponding to Table A20, averaged over all simulation iterations and path points, shown with standard errors.

METHOD	TYPE	CARDINALITY			INPUT PROPORTION		
		\mathcal{A}_v	\mathcal{C}_v	\mathcal{O}_v	\mathcal{K}_v	$\mathcal{O}_v / \mathcal{A}_v$	\mathcal{O}_v / p
DFR-ASGL	ORDER 2	40.6 ± 0.4	33.1 ± 0.3	72.1 ± 0.7	0.081 ± 0.004	1.773 ± 0.007	0.034 ± 0.0003
DFR-SGL	ORDER 2	40.8 ± 0.4	41.0 ± 0.4	80.1 ± 0.8	0 ± 0	1.951 ± 0.009	0.038 ± 0.0004
SPARSEGL	ORDER 2	40.8 ± 0.4	566.4 ± 6.2	566.4 ± 6.2	-	13.026 ± 0.075	0.268 ± 0.0030
DFR-ASGL	ORDER 3	74.1 ± 1.0	97.7 ± 1.2	168.7 ± 2.0	0.058 ± 0.004	2.405 ± 0.025	0.023 ± 0.0003
DFR-SGL	ORDER 3	82.7 ± 1.1	145.3 ± 1.8	224.2 ± 2.8	0 ± 0	2.829 ± 0.025	0.031 ± 0.0004
SPARSEGL	ORDER 3	82.8 ± 1.1	1883.4 ± 25.2	1883.4 ± 25.2	-	20.204 ± 0.184	0.257 ± 0.0030

Table A23: Model fitting metrics corresponding to Table A20, averaged over all simulation iterations and path points, shown with standard errors.

METHOD	TYPE	TIMINGS			ITERATIONS			ℓ_2 DISTANCE			FAILED CONVERGENCE		
		NO SCREEN (S)	SCREEN (S)	IMPROVEMENT FACTOR	NO SCREEN	SCREEN	TO NO SCREEN	TO NO SCREEN	NO SCREEN	SCREEN	NO SCREEN	SCREEN	
DFR-ASGL	ORDER 2	357 ± 22	68 ± 5	7 ± 0.4	306 ± 15	150 ± 4	2×10^{-9}	1×10^{-10}	0 ± 0	0 ± 0	0 ± 0	0 ± 0	
DFR-SGL	ORDER 2	253 ± 13	45 ± 2	6 ± 0.2	326 ± 18	166 ± 5	7×10^{-10}	1×10^{-11}	0 ± 0	0 ± 0	0 ± 0	0 ± 0	
SPARSEGL	ORDER 2	253 ± 13	367 ± 30	1 ± 0.1	326 ± 18	197 ± 12	1×10^{-9}	2×10^{-11}	0 ± 0	0 ± 0	0 ± 0	0 ± 0	
DFR-ASGL	ORDER 3	2425 ± 198	208 ± 10	12 ± 1.0	835 ± 57	358 ± 12	2×10^{-9}	8×10^{-11}	0 ± 0	0 ± 0	0 ± 0	0 ± 0	
DFR-SGL	ORDER 3	1077 ± 91	134 ± 8	8 ± 0.4	844 ± 62	451 ± 19	5×10^{-10}	1×10^{-11}	0 ± 0	0 ± 0	0 ± 0	0 ± 0	
SPARSEGL	ORDER 3	1077 ± 91	1167 ± 156	2 ± 0.3	844 ± 62	561 ± 43	5×10^{-10}	2×10^{-11}	0 ± 0	0 ± 0	0 ± 0	0 ± 0	

Table A24: Group screening metrics corresponding to Figures A8 (left) and A9 (left), averaged over all simulation iterations, sparsity proportion cases, and path points, shown with standard errors.

METHOD	CARDINALITY			INPUT PROPORTION		
	\mathcal{A}_g	C_g	\mathcal{O}_g	\mathcal{K}_g	$\mathcal{O}_g / \mathcal{A}_g$	\mathcal{O}_g / m
DFR-ASGL	9.09 ± 0.03	9.87 ± 0.03	9.88 ± 0.03	-	1.1033 ± 0.0011	0.4489 ± 0.0015
DFR-SGL	9.39 ± 0.03	10.41 ± 0.03	10.41 ± 0.03	-	1.1348 ± 0.0013	0.4733 ± 0.0016
SPARSEGL	9.39 ± 0.03	9.75 ± 0.03	9.75 ± 0.03	0 ± 0	$1.0344 \pm 8 \times 10^{-4}$	0.4433 ± 0.0015

Table A25: Variable screening metrics corresponding to Figures A8 (left) and A9 (left), averaged over all simulation iterations, sparsity proportion cases, and path points, shown with standard errors.

METHOD	CARDINALITY			INPUT PROPORTION		
	\mathcal{A}_v	C_v	\mathcal{O}_v	\mathcal{K}_v	$\mathcal{O}_v / \mathcal{A}_v$	\mathcal{O}_v / p
DFR-ASGL	49.61 ± 0.2	21.32 ± 0.07	68.74 ± 0.26	$0.0211 \pm 7 \times 10^{-4}$	1.4654 ± 0.0021	$0.0687 \pm 3 \times 10^{-4}$
DFR-SGL	53.19 ± 0.21	24.26 ± 0.08	75.07 ± 0.28	0 ± 0	1.4990 ± 0.0022	$0.0751 \pm 3 \times 10^{-4}$
SPARSEGL	53.19 ± 0.21	486.18 ± 1.66	486.18 ± 1.66	-	12.231 ± 0.0381	0.4862 ± 0.0017

Table A26: Model fitting metrics corresponding to Figures A8 (left) and A9 (left), averaged over all simulation iterations, sparsity proportion cases, and path points, shown with standard errors.

METHOD	TIMINGS			ITERATIONS			ℓ_2 DISTANCE			FAILED CONVERGENCE		
	NO SCREEN (S)	SCREEN (S)	IMPROVEMENT FACTOR	NO SCREEN	SCREEN	SCREEN	TO NO SCREEN	NO SCREEN	SCREEN	NO SCREEN	NO SCREEN	SCREEN
DFR-ASGL	41.4 ± 0.8	21.2 ± 0.4	2.9 ± 0.1	57.9 ± 0.4	40.6 ± 0.4	$8 \times 10^{-10} \pm 4 \times 10^{-11}$	$8 \times 10^{-10} \pm 4 \times 10^{-11}$	0 ± 0	0 ± 0	0 ± 0	0 ± 0	0 ± 0
DFR-SGL	48.6 ± 1.0	24.5 ± 0.5	2.9 ± 0.1	64.0 ± 0.4	43.9 ± 0.4	$1 \times 10^{-10} \pm 3 \times 10^{-12}$	$1 \times 10^{-10} \pm 3 \times 10^{-12}$	0 ± 0	0 ± 0	0 ± 0	0 ± 0	0 ± 0
SPARSEGL	48.6 ± 1.0	46.2 ± 0.9	1.6 ± 0.1	64.0 ± 0.4	63.6 ± 0.4	$5 \times 10^{-11} \pm 2 \times 10^{-12}$	$5 \times 10^{-11} \pm 2 \times 10^{-12}$	0 ± 0	0 ± 0	0 ± 0	0 ± 0	0 ± 0

Table A27: Group screening metrics corresponding to Figures A8 (right) and A9 (right), averaged over all simulation iterations, signal strength cases, and path points, shown with standard errors.

METHOD	CARDINALITY				INPUT PROPORTION			
	\mathcal{A}_g	\mathcal{C}_g	\mathcal{O}_g	\mathcal{K}_g	$\mathcal{O}_g / \mathcal{A}_g$	$\mathcal{O}_g / \mathcal{A}_g$	\mathcal{O}_g / m	
DFR-ASGL	5.77 ± 0.02	6.04 ± 0.02	6.04 ± 0.02	-	1.0242 ± 0.0012	1.0242 ± 0.0012	0.2746 ± 0.001	
DFR-SGL	5.80 ± 0.02	6.29 ± 0.02	6.29 ± 0.02	-	1.0564 ± 0.0014	1.0564 ± 0.0014	0.2857 ± 0.0011	
SPARSEGL	5.80 ± 0.02	5.71 ± 0.02	5.71 ± 0.02	$2 \times 10^{-5} \pm 2 \times 10^{-5}$	$0.9562 \pm 1 \times 10^{-3}$	$0.9562 \pm 1 \times 10^{-3}$	$0.2594 \pm 1 \times 10^{-3}$	

Table A28: Variable screening metrics corresponding to Figures A8 (right) and A9 (right), averaged over all simulation iterations, signal strength cases, and path points, shown with standard errors.

METHOD	CARDINALITY				INPUT PROPORTION			
	\mathcal{A}_v	\mathcal{C}_v	\mathcal{O}_v	\mathcal{K}_v	$\mathcal{O}_v / \mathcal{A}_v$	$\mathcal{O}_v / \mathcal{A}_v$	\mathcal{O}_v / p	
DFR-ASGL	42.22 ± 0.12	20.54 ± 0.05	61.10 ± 0.15	$0.0142 \pm 5 \times 10^{-4}$	1.5138 ± 0.0014	1.5138 ± 0.0014	$0.0611 \pm 2 \times 10^{-4}$	
DFR-SGL	45.32 ± 0.12	23.19 ± 0.06	66.78 ± 0.16	0 ± 0	1.5277 ± 0.0014	1.5277 ± 0.0014	$0.0668 \pm 2 \times 10^{-4}$	
SPARSEGL	45.33 ± 0.12	290.29 ± 1.07	290.29 ± 1.07	-	6.2306 ± 0.0152	6.2306 ± 0.0152	0.2903 ± 0.0011	

Table A29: Model fitting metrics corresponding to Figures A8 (right) and A9 (right), averaged over all simulation iterations, signal strength cases, and path points, shown with standard errors.

METHOD	TIMINGS			ITERATIONS			ℓ_2 DISTANCE			FAILED CONVERGENCE		
	NO SCREEN (S)	SCREEN (S)	IMPROVEMENT FACTOR	NO SCREEN	SCREEN	SCREEN	TO NO SCREEN	NO SCREEN	SCREEN	NO SCREEN	NO SCREEN	SCREEN
DFR-ASGL	50.9 ± 1.0	21.8 ± 0.5	3.4 ± 0.1	68.2 ± 0.6	51.0 ± 0.4	51.0 ± 0.4	$1 \times 10^{-9} \pm 5 \times 10^{-11}$	$1 \times 10^{-9} \pm 5 \times 10^{-11}$	$1 \times 10^{-9} \pm 5 \times 10^{-11}$	0 ± 0	0 ± 0	0 ± 0
DFR-SGL	46.0 ± 0.8	20.0 ± 0.4	3.5 ± 0.1	76.3 ± 0.7	56.2 ± 0.5	56.2 ± 0.5	$8 \times 10^{-11} \pm 1 \times 10^{-12}$	$8 \times 10^{-11} \pm 1 \times 10^{-12}$	$8 \times 10^{-11} \pm 1 \times 10^{-12}$	0 ± 0	0 ± 0	0 ± 0
SPARSEGL	46.0 ± 0.8	38.8 ± 0.7	1.7 ± 0.1	76.3 ± 0.7	63.5 ± 0.5	63.5 ± 0.5	$8 \times 10^{-11} \pm 9 \times 10^{-13}$	$8 \times 10^{-11} \pm 9 \times 10^{-13}$	$8 \times 10^{-11} \pm 9 \times 10^{-13}$	0 ± 0	0 ± 0	0 ± 0

Table A30: Group screening metrics corresponding to Figures A10 (left) and A11 (left), averaged over all simulation iterations, correlation cases, and path points, shown with standard errors.

METHOD	CARDINALITY				INPUT PROPORTION			
	$\mathcal{A}_g \downarrow$	\mathcal{C}_g	\mathcal{O}_g	\mathcal{K}_g	$\mathcal{O}_g / \mathcal{A}_g$	\mathcal{O}_g / m		
DFR-ASGL	7.46 ± 0.03	7.90 ± 0.03	7.91 ± 0.03	–	1.0379 ± 0.0012	0.3594 ± 0.0013		
DFR-SGL	7.58 ± 0.03	8.20 ± 0.03	8.20 ± 0.03	–	1.0529 ± 0.0013	0.3726 ± 0.0014		
SPARSEGL	7.58 ± 0.03	7.64 ± 0.03	7.64 ± 0.03	$2 \times 10^{-4} \pm 6 \times 10^{-5}$	$0.967 \pm 1 \times 10^{-3}$	0.3473 ± 0.0013		

Table A31: Variable screening metrics corresponding to Figures A10 (left) and A11 (left), averaged over all simulation iterations, correlation cases, and path points, shown with standard errors.

METHOD	CARDINALITY				INPUT PROPORTION			
	\mathcal{A}_v	\mathcal{C}_v	\mathcal{O}_v	\mathcal{K}_v	$\mathcal{O}_v / \mathcal{A}_v$	\mathcal{O}_v / p		
DFR-ASGL	41.78 ± 0.15	24.28 ± 0.07	64.35 ± 0.20	6×10^{-4}	1.6487 ± 0.0022	$0.0643 \pm 2 \times 10^{-4}$		
DFR-SGL	45.89 ± 0.16	27.01 ± 0.08	71.04 ± 0.22	0 ± 0	1.6442 ± 0.0023	$0.071 \pm 2 \times 10^{-4}$		
SPARSEGL	45.89 ± 0.16	379.16 ± 1.50	379.17 ± 1.50	–	9.3997 ± 0.0307	0.3792 ± 0.0015		

Table A32: Model fitting metrics corresponding to Figures A10 (left) and A11 (left), averaged over all simulation iterations, correlation cases, and path points, shown with standard errors.

METHOD	TIMINGS			ITERATIONS			ℓ_2 DISTANCE			FAILED CONVERGENCE		
	No SCREEN (s)	SCREEN (s)	IMPROVEMENT FACTOR	No SCREEN	SCREEN	SCREEN	To NO SCREEN	NO SCREEN	SCREEN	No SCREEN	NO SCREEN	SCREEN
DFR-ASGL	86.0 ± 3.4	21.7 ± 0.4	3.8 ± 0.1	132.5 ± 6.1	73.3 ± 1.8	$1 \times 10^{-9} \pm 5 \times 10^{-11}$	$1 \times 10^{-9} \pm 5 \times 10^{-11}$	0 ± 0	0 ± 0	0 ± 0	0 ± 0	0 ± 0
DFR-SGL	97.4 ± 4.2	24.4 ± 0.5	4.0 ± 0.2	145.3 ± 6.5	79.9 ± 2.1	$2 \times 10^{-10} \pm 2 \times 10^{-12}$	$2 \times 10^{-10} \pm 2 \times 10^{-12}$	0 ± 0	0 ± 0	0 ± 0	0 ± 0	0 ± 0
SPARSEGL	97.4 ± 4.2	66.2 ± 1.7	1.8 ± 0.1	145.3 ± 6.5	132.2 ± 4.8	$3 \times 10^{-11} \pm 7 \times 10^{-13}$	$3 \times 10^{-11} \pm 7 \times 10^{-13}$	0 ± 0	0 ± 0	0 ± 0	0 ± 0	0 ± 0

Table A33: Group screening metrics corresponding to Figures A10 (right) and A11 (right), averaged over all simulation iterations, α cases, and path points, shown with standard errors.

METHOD	CARDINALITY			INPUT PROPORTION		
	\mathcal{A}_g	\mathcal{C}_g	\mathcal{O}_g	\mathcal{K}_g	$\mathcal{O}_g / \mathcal{A}_g$	\mathcal{O}_g / m
DFR-ASGL	8.41 ± 0.03	7.86 ± 0.03	7.86 ± 0.03	-	0.8905 ± 0.0013	0.3571 ± 0.0013
DFR-SGL	9.73 ± 0.03	9.30 ± 0.03	9.31 ± 0.03	-	0.9128 ± 0.0012	0.4230 ± 0.0013
SPARSEGL	9.74 ± 0.03	10.02 ± 0.03	10.02 ± 0.03	0 ± 0	1.3212 ± 0.011	0.4557 ± 0.0014

Table A34: Variable screening metrics corresponding to Figures A10 (right) and A11 (right), averaged over all simulation iterations, α cases, and path points, shown with standard errors.

METHOD	CARDINALITY			INPUT PROPORTION		
	\mathcal{A}_v	\mathcal{C}_v	\mathcal{O}_v	\mathcal{K}_v	$\mathcal{O}_v / \mathcal{A}_v$	\mathcal{O}_v / p
DFR-ASGL	179.90 ± 0.77	65.84 ± 0.31	238.58 ± 0.99	$9 \times 10^{-4} \pm 1 \times 10^{-4}$	1.3751 ± 0.0025	$0.2386 \pm 1 \times 10^{-3}$
DFR-SGL	186.76 ± 0.79	72.25 ± 0.34	251.18 ± 1.03	$4 \times 10^{-5} \pm 3 \times 10^{-5}$	1.3891 ± 0.0026	0.2512 ± 0.0010
SPARSEGL	186.86 ± 0.79	467.06 ± 1.51	467.07 ± 1.51	-	17.1921 ± 0.3909	0.4671 ± 0.0015

Table A35: Model fitting metrics corresponding to Figures A10 (right) and A11 (right), averaged over all simulation iterations, α cases, and path points, shown with standard errors.

METHOD	TIMINGS (S)			ITERATIONS			ℓ_2 DISTANCE			FAILED CONVERGENCE		
	NO SCREEN	SCREEN	IMPROVEMENT FACTOR	NO SCREEN	SCREEN		TO NO SCREEN	NO SCREEN	SCREEN	NO SCREEN	NO SCREEN	SCREEN
DFR-ASGL	101.5 ± 2.1	51.9 ± 1.3	2.2 ± 0.02	152.7 ± 2.5	112.5 ± 2.1		$1 \times 10^{-10} \pm 2 \times 10^{-11}$	0 ± 0	0 ± 0	0 ± 0	0 ± 0	0 ± 0
DFR-SGL	107.8 ± 1.9	55.1 ± 1.4	2.7 ± 0.05	186.8 ± 2.8	123.8 ± 1.9		$2 \times 10^{-10} \pm 4 \times 10^{-11}$	0 ± 0	0 ± 0	0 ± 0	0 ± 0	0 ± 0
SPARSEGL	107.8 ± 1.9	152.7 ± 4.2	1.0 ± 0.02	186.8 ± 2.8	169.5 ± 2.9		$4 \times 10^{-11} \pm 6 \times 10^{-13}$	0 ± 0	0 ± 0	0 ± 0	0 ± 0	0 ± 0

D.7 Cross-validation

Cross-validation (CV) is an important tool for tuning λ . However, due to its cost, α is often set manually, rather than included in a grid optimization scheme. Using DFR with 10-fold CV yielded computationally gains (Table A36) that enable future tuning schemes for SGL to consider both α and λ , and aSGL to include the weight hyper-parameters γ_1 and γ_2 .

Table A36: The *improvement factor* for the screening methods applied to synthetic data, under the linear and logistic models, with cross-validation (CV), with standard errors. The data was generated using the parameters in Table A1.

Method	Linear	Logistic
DFR-aSGL	3.9 ± 0.2	2.3 ± 0.1
DFR-SGL	4.2 ± 0.3	2.6 ± 0.1
sparsegl	2.0 ± 0.2	2.1 ± 0.1

E Real data analysis

E.1 Data description

- **brca1**: Gene expression data for breast cancer tissue samples.
 - Response (continuous): Gene expression measurements for the BRCA1 gene.
 - Data matrix: Gene expression measurements for the other genes.
 - Grouping structure: Variables are grouped via singular value decomposition.
- **scheetz**: Gene expression data in the mammalian eye.
 - Response (continuous): Gene expression measurements for the Trim32 gene.
 - Data matrix: Gene expression measurements for the other genes.
 - Grouping structure: Variables are grouped via singular value decomposition.
- **trust-experts**: Survey response data as to how much participants trust "experts" (e.g. doctors, nurses, scientists) to provide COVID-19 news and information.
 - Response (continuous): The trust level of each participant.
 - Data matrix: Contingency table including factors about participants (e.g. age, gender, ethnicity).
 - Grouping structure: The factor levels grouped into their original factors.
- **adenoma**: Transcriptome profile data to identify the formation of colorectal adenomas, which are the predominate cause of colorectal cancers.
 - Response (binary): Labels classifying whether the sample came from an adenoma or normal mucosa.
 - Data matrix: Transcriptome profile measurements.
 - Grouping structure: Genes were assigned to pathways from all nine gene sets on the Molecular Signature Database.
- **celiac**: Gene expression data of primary leucocytes to identify celiac disease.
 - Response (binary): Labels classifying patients into whether they have celiac disease.
 - Data matrix: Gene expression measurements from the primary leucocytes.
 - Grouping structure: Genes were assigned to pathways from all nine gene sets on the Molecular Signature Database.
- **tumour**: Gene expression data of pancreatic cancer samples to identify tumorous tissue.
 - Response (binary): Labels classifying whether sample is from normal of tumour tissue.
 - Data matrix: Gene expression measurements.
 - Grouping structure: Genes were assigned to pathways from all nine gene sets on the Molecular Signature Database.

Table A37: Dataset information for the six datasets used in the real data analysis.

Dataset	p	n	m	Group sizes	Type	Source
brca1	17322	536	243	[1, 6505]	Linear	[20] ¹
scheetz	18975	120	85	[1, 6274]	Linear	[39] ¹
trust-experts	101	9759	7	[4, 51]	Linear	[38] ²
adenoma	18559	64	313	[1, 741]	Logistic	[37] ³
celiac	14657	132	276	[1, 617]	Logistic	[17] ³
tumour	18559	52	313	[1, 741]	Logistic	[34, 25, 10] ³

¹downloaded from <https://iowabiostat.github.io/data-sets/>

²downloaded from <https://github.com/dajmcdon/sparsegl>

³downloaded from <https://www.ncbi.nlm.nih.gov/>

E.2 Additional results for the real data

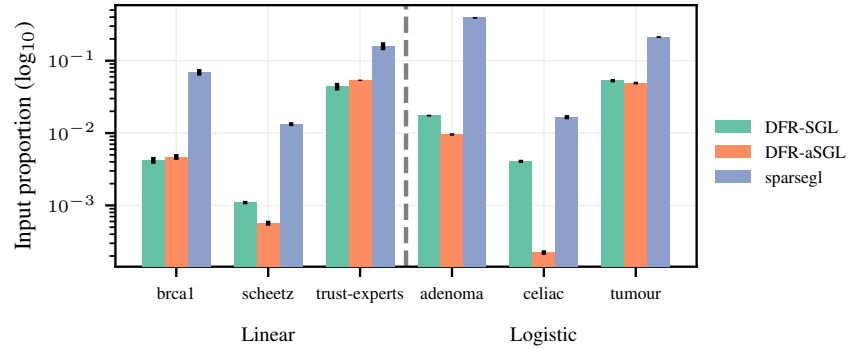


Figure A12: The *input proportion* (log₁₀ scale) of the screening methods applied to the six real datasets, split into the model type.

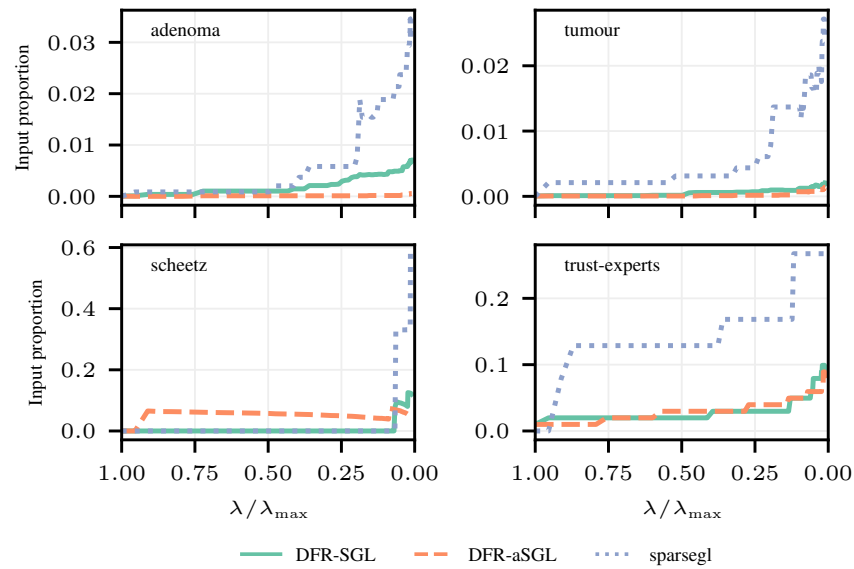


Figure A13: The *input proportion* as a function of the shrinkage path for the screening methods applied to the *adenoma*, *tumour*, *scheetz*, and *trust-experts* datasets.

Table A38: Group screening metrics corresponding to Figure 4 averaged over all path points, shown with standard errors.

METHOD	DATASET	CARDINALITY			INPUT PROPORTION		
		\mathcal{A}_g	\mathcal{C}_g	\mathcal{O}_g	\mathcal{K}_g	$\mathcal{O}_g / \mathcal{A}_g$	\mathcal{O}_g / m
DFR-ASGL	ADENOMA	0.86 ± 0.06	0.84 ± 0.06	0.87 ± 0.07	-	1.0069 ± 0.0069	$0.0028 \pm 2 \times 10^{-4}$
DFR-SGL	ADENOMA	3.30 ± 0.21	13.46 ± 0.68	13.46 ± 0.68	-	4.6121 ± 0.2003	0.0430 ± 0.0022
SPARSEGL	ADENOMA	3.32 ± 0.21	158.61 ± 14.9	8.59 ± 0.53	0 ± 0	2.6141 ± 0.0942	0.0274 ± 0.0017
DFR-ASGL	CELIAC	5.71 ± 0.73	8.95 ± 1.21	8.61 ± 1.14	-	1.3943 ± 0.0374	0.0312 ± 0.0041
DFR-SGL	CELIAC	15.35 ± 1.45	22.04 ± 2.03	22.04 ± 2.03	-	1.4367 ± 0.0276	0.0799 ± 0.0074
SPARSEGL	CELIAC	15.36 ± 1.46	519.23 ± 64.07	19.32 ± 1.84	0 ± 0	1.2415 ± 0.0213	0.0700 ± 0.0067
DFR-ASGL	BC-TGCA	2.04 ± 0.16	2.04 ± 0.16	2.06 ± 0.16	-	1.0089 ± 0.0062	$0.0085 \pm 7 \times 10^{-4}$
DFR-SGL	BC-TGCA	5.60 ± 0.48	6.90 ± 0.60	6.90 ± 0.60	-	1.2023 ± 0.0218	0.0284 ± 0.0025
SPARSEGL	BC-TGCA	5.59 ± 0.48	3384.28 ± 258.04	6.25 ± 0.55	0 ± 0	1.1062 ± 0.0176	0.0257 ± 0.0022
DFR-ASGL	SHEETZ	0.16 ± 0.04	0.16 ± 0.04	0.16 ± 0.04	-	1.0000 ± 0.0000	$0.0019 \pm 4 \times 10^{-4}$
DFR-SGL	SHEETZ	0.61 ± 0.08	0.86 ± 0.12	0.86 ± 0.12	-	1.3537 ± 0.0531	0.0101 ± 0.0014
SPARSEGL	SHEETZ	0.61 ± 0.08	1515.48 ± 220.52	0.73 ± 0.10	0 ± 0	1.1829 ± 0.0486	0.0086 ± 0.0012
DFR-ASGL	TRUST-EXPERTS	5.43 ± 0.13	5.43 ± 0.13	5.45 ± 0.13	-	1.0040 ± 0.0028	0.7792 ± 0.0187
DFR-SGL	TRUST-EXPERTS	6.29 ± 0.12	6.32 ± 0.12	6.32 ± 0.12	-	1.0067 ± 0.0053	0.9033 ± 0.0169
SPARSEGL	TRUST-EXPERTS	6.25 ± 0.12	0.39 ± 0.28	6.25 ± 0.12	0 ± 0	1.0000 ± 0.0000	0.8932 ± 0.0174
DFR-ASGL	TUMOUR	2.07 ± 0.16	2.66 ± 0.24	2.69 ± 0.24	-	1.2173 ± 0.0317	$0.0086 \pm 8 \times 10^{-4}$
DFR-SGL	TUMOUR	5.02 ± 0.24	8.80 ± 0.38	8.80 ± 0.38	-	1.8253 ± 0.0357	0.0281 ± 0.0012
SPARSEGL	TUMOUR	5.02 ± 0.24	126.78 ± 11.49	6.77 ± 0.29	0 ± 0	1.4276 ± 0.0351	$0.0216 \pm 9 \times 10^{-4}$

Table A39: Variable screening metrics corresponding to Figure 4 averaged over all path points, shown with standard errors.

METHOD	DATASET	CARDINALITY					INPUT PROPORTION		
		\mathcal{A}_v	\mathcal{C}_v	\mathcal{O}_v	\mathcal{K}_v	$\mathcal{O}_v / \mathcal{A}_v$	\mathcal{O}_v / p		
DFR-ASGL	ADENOMA	1.95 ± 0.15	0.23 ± 0.06	2.16 ± 0.18	0.0303 ± 0.0173	1.1083 ± 0.0261	$1 \times 10^{-4} \pm 1 \times 10^{-5}$		
DFR-SGL	ADENOMA	14.38 ± 1.11	61.47 ± 2.90	75.51 ± 3.85	0 ± 0	8.9655 ± 0.7776	$0.0041 \pm 2 \times 10^{-4}$		
SPARSEGL	ADENOMA	14.41 ± 1.12	308.64 ± 20.81	308.64 ± 20.81	–	26.0099 ± 1.6361	0.0166 ± 0.0011		
DFR-ASGL	CELIAC	9.58 ± 1.49	7.48 ± 1.12	16.63 ± 2.47	0.0707 ± 0.0259	1.6234 ± 0.0667	$0.0011 \pm 2 \times 10^{-4}$		
DFR-SGL	CELIAC	37.13 ± 3.92	26.11 ± 3.05	61.94 ± 6.77	0 ± 0	1.6187 ± 0.0455	$0.0042 \pm 5 \times 10^{-4}$		
SPARSEGL	CELIAC	37.26 ± 3.94	1019.13 ± 106.78	1019.13 ± 106.78	–	27.6753 ± 1.1176	0.0695 ± 0.0073		
DFR-ASGL	BC-TGCA	97.41 ± 6.95	20.63 ± 2.36	116.59 ± 8.33	0.0202 ± 0.0142	1.1741 ± 0.0088	$0.0067 \pm 5 \times 10^{-4}$		
DFR-SGL	BC-TGCA	241.69 ± 7.34	63.42 ± 4.26	301.80 ± 8.81	0 ± 0	3.9386 ± 2.6945	$0.0174 \pm 5 \times 10^{-4}$		
SPARSEGL	BC-TGCA	241.59 ± 7.34	6762.31 ± 186.59	6762.31 ± 186.59	–	95.8171 ± 66.0170	0.3904 ± 0.0108		
DFR-ASGL	SCHEETZ	136.1 ± 31.35	56.07 ± 15.33	184.25 ± 42.43	0 ± 0	1.3543 ± 0.0065	0.0097 ± 0.0022		
DFR-SGL	SCHEETZ	501.78 ± 60.68	344.92 ± 50.24	836.23 ± 101.02	0 ± 0	1.6688 ± 0.0651	0.0441 ± 0.0053		
SPARSEGL	SCHEETZ	501.49 ± 60.66	3030.24 ± 385.6	3030.24 ± 385.60	–	6.1978 ± 0.3472	0.1597 ± 0.0203		
DFR-ASGL	TRUST-EXPERTS	18.04 ± 1.11	0.82 ± 0.12	18.58 ± 1.14	0.0202 ± 0.0142	1.0315 ± 0.0064	0.1839 ± 0.0113		
DFR-SGL	TRUST-EXPERTS	33.88 ± 1.88	1.29 ± 0.13	34.62 ± 1.89	0 ± 0	1.0277 ± 0.0055	0.3427 ± 0.0187		
SPARSEGL	TRUST-EXPERTS	33.77 ± 1.89	0.75 ± 0.56	79.64 ± 3.19	–	2.6808 ± 0.0742	0.7885 ± 0.0315		
DFR-ASGL	TUMOUR	3.20 ± 0.35	1.67 ± 0.27	4.77 ± 0.57	0.0303 ± 0.0173	1.3084 ± 0.0523	$3 \times 10^{-4} \pm 3 \times 10^{-5}$		
DFR-SGL	TUMOUR	10.70 ± 0.72	9.87 ± 0.50	20.34 ± 1.09	0 ± 0	2.3432 ± 0.1189	$0.0011 \pm 6 \times 10^{-5}$		
SPARSEGL	TUMOUR	10.70 ± 0.72	246.80 ± 15.39	246.80 ± 15.39	–	25.9945 ± 0.9193	$0.0133 \pm 8 \times 10^{-4}$		

Table A40: Model fitting metrics corresponding to Figure 4 averaged over all path points, shown with standard errors. There are no standard errors for the timing results as the time to calculate the whole path was evaluated.

METHOD	DATASET	TIMINGS			ITERATIONS			ℓ_2 DISTANCE			FAILED CONVERGENCE	
		NO SCREEN (S)	SCREEN (S)	I.F.	NO SCREEN	SCREEN	SCREEN	TO NO SCREEN	NO SCREEN	SCREEN	NO SCREEN	SCREEN
DFR-ASGL	ADENOMA	6404.87	6.98	917.60	6647.43 ± 446.54	39.78 ± 7.08	5 × 10 ⁻⁵ ± 5 × 10 ⁻⁶	0.61 ± 0.05	0.00 ± 0.00			
DFR-SGL	ADENOMA	9017.70	149.10	60.48	9272.9 ± 205.31	4374.64 ± 286.62	3 × 10 ⁻⁵ ± 2 × 10 ⁻⁶	0.87 ± 0.03	0.00 ± 0.00			
SPARSEGL	ADENOMA	9017.70	198.36	45.46	9272.9 ± 205.31	5140.16 ± 390.91	3 × 10 ⁻⁵ ± 2 × 10 ⁻⁶	0.87 ± 0.03	0.04 ± 0.02			
DFR-ASGL	CELIAC	990.00	7.07	140.01	854.09 ± 104.75	28.55 ± 3.45	3 × 10 ⁻⁸ ± 4 × 10 ⁻⁹	0.00 ± 0.00	0.00 ± 0.00			
DFR-SGL	CELIAC	1391.78	10.31	134.95	1195.34 ± 98.13	75.37 ± 9.60	2 × 10 ⁻⁷ ± 1 × 10 ⁻⁸	0.00 ± 0.00	0.00 ± 0.00			
SPARSEGL	CELIAC	1391.78	16.49	84.40	1195.34 ± 98.13	93.29 ± 8.86	8 × 10 ⁻⁸ ± 3 × 10 ⁻⁹	0.00 ± 0.00	0.00 ± 0.00			
DFR-ASGL	BC-TGCA	16838.53	116.19	144.92	1264.26 ± 76.24	202.37 ± 15.62	3 × 10 ⁻⁹ ± 1 × 10 ⁻⁹	0.00 ± 0.00	0.00 ± 0.00			
DFR-SGL	BC-TGCA	22227.01	103.78	214.17	1674.07 ± 19.77	334.16 ± 13.44	2 × 10 ⁻¹² ± 3 × 10 ⁻¹³	0.00 ± 0.00	0.00 ± 0.00			
SPARSEGL	BC-TGCA	22227.01	4132.04	5.38	1674.07 ± 19.77	1580.73 ± 44.23	4 × 10 ⁻¹⁴ ± 1 × 10 ⁻¹⁴	0.00 ± 0.00	0.00 ± 0.00			
DFR-ASGL	SHEETZ	2502.89	107.91	23.19	63.26 ± 15.42	7.52 ± 1.88	3 × 10 ⁻¹⁴ ± 1 × 10 ⁻¹⁴	0.00 ± 0.00	0.00 ± 0.00			
DFR-SGL	SHEETZ	68084.77	2246.13	30.31	1891.21 ± 386.40	642.38 ± 136.12	3 × 10 ⁻⁹ ± 8 × 10 ⁻¹⁰	0.18 ± 0.04	0.00 ± 0.00			
SPARSEGL	SHEETZ	68084.77	6666.65	10.21	1891.21 ± 386.40	1890.45 ± 386.44	5 × 10 ⁻²² ± 2 × 10 ⁻²²	0.18 ± 0.04	0.18 ± 0.04			
DFR-ASGL	TRUST-EXPERTS	15.54	10.40	1.49	204.04 ± 10.17	207.31 ± 9.91	1 × 10 ⁻⁶ ± 7 × 10 ⁻⁷	0.00 ± 0.00	0.00 ± 0.00			
DFR-SGL	TRUST-EXPERTS	30.81	22.67	1.36	421.39 ± 33.70	417.06 ± 33.98	1 × 10 ⁻¹³ ± 3 × 10 ⁻¹⁴	0.00 ± 0.00	0.00 ± 0.00			
SPARSEGL	TRUST-EXPERTS	30.81	29.62	1.04	421.39 ± 33.70	433.48 ± 32.67	3 × 10 ⁻⁶ ± 2 × 10 ⁻⁶	0.00 ± 0.00	0.00 ± 0.00			
DFR-ASGL	TUMOUR	6006.52	6.67	900.39	7418.52 ± 427.11	52.22 ± 6.20	2 × 10 ⁻⁸ ± 1 × 10 ⁻⁸	0.56 ± 0.05	0.00 ± 0.00			
DFR-SGL	TUMOUR	7466.83	89.43	83.49	9272.02 ± 224.60	186.27 ± 7.64	3 × 10 ⁻⁹ ± 2 × 10 ⁻¹⁰	0.86 ± 0.04	0.00 ± 0.00			
SPARSEGL	TUMOUR	7466.83	90.03	82.93	9272.02 ± 224.60	197.4 ± 9.38	2 × 10 ⁻⁹ ± 2 × 10 ⁻¹⁰	0.86 ± 0.04	0.00 ± 0.00			